AMPEROMETRIC DETECTION OF NITRATE USING Sn-Cu_xO NANOCOMPOSITE

By

GLORIA KASONGO KIBAMBO

Thesis Submitted in fulfillment of the requirements for the degree Master of Engineering: Chemical Engineering

In the

Faculty of Engineering and Built Environment

At the

CAPE PENINSULA UNIVERSITY OF TECHNOLOGY

Supervisor: Prof Chowdhury

Bellville Campus

November 2023

Declaration

I, GLORIA KASONGO KIBAMBO, declare that the contents of this thesis represent my own unaided work, and that the thesis has not previously been submitted for academic examination towards any qualification. Furthermore, it represents my own opinions and not necessarily those of the Cape Peninsula University of Technology.

Signature:  ……..

Signed ……at Cape Town……On this……Day……of 17th November 2023……

Abstract

This thesis presents a comprehensive investigation into the structural, physical, and electrochemical characteristics of Cu_xO and Sn-doped Cu_xO nanocomposite thin films as catalysts for the amperometric detection of nitrate. Excessive Nitrate is harmful to human thus the motivation of this work. The unique electrochemical and electronic properties of Cu_xO (Cu_2O/CuO) gives it merit to be used in the development of electronic devices. The nanocomposite thin films were constructed by a simple chemical route, a two-step spin-coating method and calcination technologies. The study involves X-ray diffraction (XRD), scanning electron microscopy (SEM), and X-ray photoelectron spectroscopy (XPS) for physical characterization. The XRD analysis reveals the presence of cubic Cu_2O and monoclinic CuO phases in pristine Cu_xO, while Sn doping induces crystallographic changes. Doping with Sn led to an increase in the quantity of electron transfers, increasing from 1 to 2 when compared to undoped Cu_xO.

The electrochemical characterization, performed through cyclic voltammetry (CV), chronoa mperometry (CA), and electrochemical impedance spectroscopy (EIS) in alkaline electrolyte, evaluates the catalytic performance for nitrate detection. Sn-doped Cu_xO exhibits enhanced electro catalytic activity compared to pristine Cu_xO, attributed to the incorporation of Sn into the lattice. The developed Sn-doped Cu_xO/FTO sensor demonstrates a high sensitivity of 100.27 $\mu A.mM^{-1}.cm^{-2}$ with a low limit of detection (LOD) of 0.04 µM (S/N) = 3), a linear concentration range of up to 15 mM and a fast response time of less than 5s was observed at a potential of -1 V (vs. Ag/AgCl). The sensor shows selectivity for nitrate ions in the presence of common interfering anions. Reproducibility, stability, and shelf life assessments affirm the practical viability of the Sn-doped Cu_xO/FTO electrode. The sensing device was applied to the determination of nitrate in spiked tap water, the Mowbray River and Bore Hole water samples.

The study contributes valuable insights into the design and optimization of catalysts for electrochemical sensing applications.

Acknowledgements

I wish to thank:

- Firstly God Almighty for everything he has done for me, for being there in each and every step of this project, for my health, for giving me the courage, strength, knowledge and the opportunity to purse this research with all enthusiasm and perseverance and to finally complete this work satisfactorily after a long period. It wouldn't be possible without his presence.

- Secondly my supervisor Prof Mahabubur Raman Chowdhury for his endless care, he has been so patient with me and understandable from the beginning, for his assistance in my funding and his support in everything. I have been blessed to have Prof Chowdhury as my supervisor.

- Dr Masikini, always available when needed.

- Dr Chamier for her assistance throughout my research with the multiples tests needed.

- The staff and students of the department of chemical engineering at the Cape Peninsula University of Technology (CPUT), particularly in the functional material group for helping me and encouraging me throughout this research.

- Thirdly, my Husband Daniel Balela for his endless and continued support, for encouraging and pushing me every single day, for his love and patience.

- My brothers and sisters, Loic Kibambo, Evodie Kibambo, Stephane Kibambo, Alvin Kibambo for their support and patience.

- Last but not least, my parents, I wouldn't finish without expressing my gratitude towards them, for believing in me, their love, continued support, it wouldn't have been possible if it wasn't for their encouragement for making this opportunity possible.

The financial assistance of Prof Chowdhury and the CPUT funding department towards this research is acknowledged. Opinions expressed in this thesis and the conclusions arrived at, are those of the author, and are not necessarily to be attributed to the National Research Foundation.

Dedication

To my dearest and loving parents

Jean Baptiste Kibambo Kasokota & Clarisse Kungwa Lunvungu

I would not be the woman I am today if it was not for you.

.

To my beautiful brothers and sisters

Loic, Evodie, Stephane & Alvin Kibambo

I am forever grateful to you

To my loving Husband

Daniel Balela

I would not have chosen to share this journey with anyone else but you

To my beautiful Son

Ayaan Balela

Although it was not an easy road but you made me smile throughout and it gave me the strength I love you

Publications

Adijat Inyang, Gloria Kibambo, Maghmood Palmer, Franscious Cummings, Milua Masikini, Christopher Sunday, Mahabubur Chowdhury,Thin Solid Films, Volume 709, 2020, 138244, ISSN 0040-6090, https://doi.org/10.1016/j.tsf.2020.138244

Ariel Ndala, Gloria Kibambo, Orlette Mkhari, Mahabubur R. Chowdhury, Two Electron Transfer Mediated Enhanced Electrochemical Nitrate Detection by Sn Doped CuxO Thin Film Electrode. Available at SSRN: http://dx.doi.org/10.2139/ssrn.4369507

Table of contents

List of tables

List of figures

List of symbols

Symbol	Description	Units
θ	incident angle or phase angle	°
λ	beam wavelength	nm
k^0	electron-transfer rate constant	sec^{-1}
α_c	transfer coefficient	C
n_c	number of electrons transferred	e^-
Γ	surface concentration	mM
R	Gas constant	J mol-1 k-1
$E^{0\prime}$	formal electrode potential	V
T	Temperature	K
F	Faraday's law constant	°C
v	scan rate	V/s
$I_{PC/1}$	cathodic peak currents	mA/cm^2
$Q_{c/1}$	integrated peak areas	cm^2

Abbreviations and Acronyms

AE	Auxiliary electrode
Au	Gold
C_{dl}	Capacitance
CE	Counter electrode
Cu	Copper
CV	Cyclic voltammetry
DPV	Differential pulse voltammetry
EIS	Electrochemical impedance spectroscopy
EPA	Environmental Protection Agency
FTO	Fluorine doped tin oxide
Gr	Graphene
LOD	Limit of detection
LSV	linear sweep voltammetry
N	Nitrogen
NCs	Nanocrystals
NO_3^-	Nitrate
NPs	Nanoparticles
NWs	Nanowires
P	Phosphorus
PPy	Polypyrrole
RE	Reference electrode
R_e	Resistance
RSD	Relative standard deviation
R_t	Charge transfer resistance
S/N	Signal to noise ratio
SEM	scanning electron microscopy
Sn	Tin
SWV	Square voltammetry
TEM	Transmission electron microscopy
WE	Working electrode
WHO	World Health Organization
XPS	X-ray Photoelectron Spectroscopy
XRD	X-ray diffraction analysis
Z	Impedance
Z_w	Charge transfer impedance

Glossary: Terms and Concepts

Amperometry involves setting an applied potential to the working electrode (Heydari et al., 2016).

Analyte is a specific substance for which testing is performed in a laboratory (Saberian-Borujeni et al., 2014).

Catalyst: a substance that increases the rate of a chemical reaction without itself undergoing any permanent chemical change (Studer and Curran, 2014).

Copper oleate is a solid complex deeply coloured a copper-blue with the odour of oleic acid. It has no definite melting point and fuses below 100°C (Whitmore and Lauro, 2002).

Cyclic voltammetry is one of the most method used for obtaining information about electrochemical reactions, electron transfer between species and the thermodynamics of redox reactions (Heydari et al., 2016).

Fluorine doped tin oxide (FTO) is a thin film transparent conducting oxide that is typically used as electrode (Heydari et al., 2016).

Nanoparticles are tiny particles that have a dimension of less than 100 nm (Adlakha-Hutcheon et al., 2009).

Nanotechnology is a field that describes materials, systems or processes that exist or operate at an extremely small scale (Vaddiraju et al., 2010).

Sensors are small devices used to detect, indicate or measure a physical property (Adlakha-Hutcheon et al., 2009).

Chapter 1 : Introduction

1.1 Introduction

Nitrates (NO_3^-) are compound that contains nitrogen and oxygen. They appear as inorganic in nature and are one of the most commonly found contaminants (i.e. arsenic, fluoride, phosphor, etc.) in surface or groundwater globally (Gutiérrez et al., 2018). Nitrates are generally found in animal wastes, septic tanks, industrial wastes, etc. But nitrogen fertilizers are the most source of contaminants into the environment (Alam et al., 2015). The problem with nitrate is when exposed to high concentrations especially in water, it may cause severe illness in adults and infants due to their interference with oxygen in the human blood. And because of the potential damage for human health, some countries and organizations have imposed limitations for nitrate concentration in potable water. The World Health Organization (WHO) (WHO, 2011) set the safe limit of nitrate in potable water to be 50 mg NO_3^-/L (WHO, 2011), Whereas Italian regulations reported it to be 45 mg NO_3^-/L and 10 mg NO_3^-/L for infants while the United States Environmental Protection Agency (EPA) recommends 44.2 mg NO_3^-/L (Amali et al., 2021). Due to this toxic aspect, it is essential to monitor the level of nitrates.

Over the last years, this issue has drawn much attention in the research area. In Southern Africa, regions including Botswana, Namibia and South Africa, suffer from groundwater contamination of nitrate and that the concentration exceeds drinking water specifications; these areas are relatively densely populated, or under agriculture (Masindi and Foteinis, 2021). At higher levels, potentially serious effects results in livestock poisoning. Studies of water quality in some of these areas of the extent of nitrate pollution observed during the past two decades show that in the northern parts of South Africa, precisely in Limpopo province, higher nitrate values were largely confined to the area with black turf oil and in the Northern Cape province, some parts of this area have a low mean annual rainfall of approximately 200mm/a resulting in a huge problem for farmers as they could not be able operate properly (Tredoux et al., 2009). At one borehole in one of the farm, a high nitrate level of 193 mg/L was recorded. In Ghanzi, the south-eastern part of Botswana, One of the borehole among other 13 boreholes tested show a high level of nitrate of 508mg/L and also in the south-eastern parts of Namibia (Claasen and Lewis, 2017). Thus, in southern Africa, excess sludge application to land and inappropriate on-site sanitation are considered the main anthropogenic sources of nitrate. There is a need to understand the level and the extent of groundwater pollution in South Africa in general but lack of data makes it difficult to achieve this goal thus a map of nitrate pollution in South Africa have been generated (Figure 1.1).

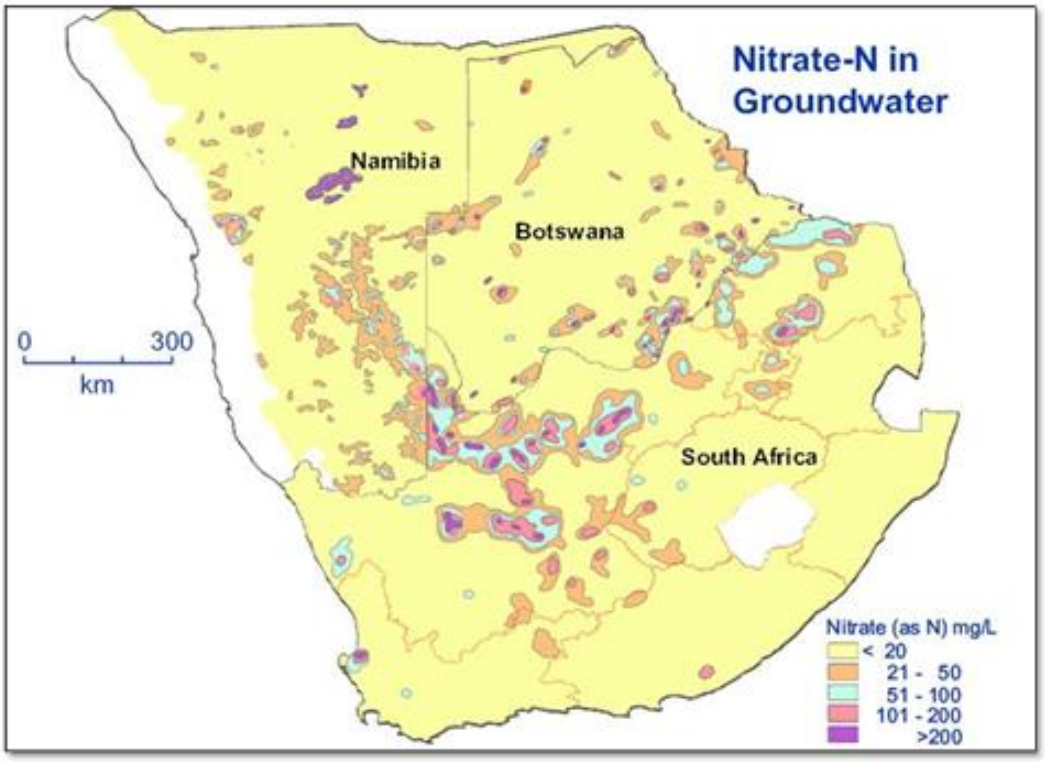

Figure 1.1: Nitrate distribution map of Southern Africa

(DWA, 2010)

In Spain, precisely in one of the provinces called Zamora, lots of pig farms are exploited in that area of Spain and the pollution from the farms poses a threat to both people and local ecosystems. Measurements (3 of them) taken on tap water to detect nitrates were all above the legal threshold established by some of the organizations listed above (Monica, 2022). In some of Spain's main pig farming regions groundwater nitrate levels have been found to be up to four times higher than the legal threshold of 50 mg per liter. While this is not so common, lower illegal levels are widespread. The tap water is contaminated and people from that area are worried because of the effect that high levels of nitrates have on human health and that includes the risk of miscarriage, birth defects and even cancer (Monica, 2022). In 2019, it was reported that the process called eutrophication led to two catastrophic events. In both cases, tons of dead fish washed ashore. Statistics shown that 23% of Spanish groundwater is contaminated by nitrates, as well as 22% of surface water (Monica, 2022). It is for the above-mentioned reasons, that nitrate reduction and determination is essential for environment and for public health issues.

Many analytical techniques are used for such purpose in different samples. That include ion-chromatography (Fu et al., 2015), spectroscopic method (Jahn et al., 2006), chemiluminescence (Kodamatani et al., 2009), Raman spectroscopy (Kim et al., 2012) etc. these methods require expensive instrumentation and wide experimental procedures. Meanwhile, electrochemical methods such as potentiometry, amperometry and voltammetry are quite selective, easy and not much cost effective. Although electroanalytical techniques do not have problems with interferences and do not require extensive pre-treatments, they however tend to suffer from poor reproducibility upon reuse of the sensor due to poisoning of the films used in them. There have been a number of report describing the mechanism of nitrate reduction in different mediums (acidic, neutral and basic) (Amali et al., 2021). According to previous studies, the reduction of nitrate is not a direct straight forward process at most commonly used electrodes. Nitrate is reduced via multiples intermediate steps. Though, numerous electrochemical studies have been reported for the reduction of nitrate ions based on the use of modification of solid electrode materials that are capable of catalyzing the reduction of nitrate (Amali et al., 2021). In recent years, non-enzymatic sensors that include nanostructures of transition metal oxides have drawn much attention from scientists and engineers due to their different properties compared with the enzymatic and have been employed in many fields of technology.

Metal oxide such as Fe_2O_3, SnO_2, TiO_2, SnO, NiO, Cu_xO and ZnO have been studied in voltammetric and amperometric sensors as catalyst for the electro reduction of nitrate (Amali et al., 2021).

Copper oxide (Cu_xO) is our material of interest. It has attracted so much attention in the research field due to its variety of unique chemical and physical properties. The subscript x in Cu_xO demonstrates the variable stoichiometry showing the different oxidation states of copper. Material containing both Cu_2O and CuO phases are referred as mixed copper oxide. These two phases differ in terms of color, electrical characteristics, and crystal structures. Cu_2O is a semiconductor with a red color caused by its bandgap structure, which enables it to absorb light in the blue and green regions of the spectrum. Some of its applications are in photovoltaic devices, photocatalysis, and electronic devices. CuO has positive charge carriers (holes) that can contribute to electronic conductivity, thus being a p-type semiconductor with a narrow bandgap of 1.2 eV, and it demonstrates antiferromagnetic properties at low temperatures. Nanostructured forms of mixed copper oxides exhibit a high surface area, leading to enhanced reactivity and catalytic performance due to the synergistic effects between different copper

oxide phases. Due to the properties and performances stated above and to the following key aspects; great thermal conductivity, photovoltaic properties, high stability, and so on, it is what making them interesting and suitable for use in various applications as catalyst such as in sensing applications, supercapacitors and electrodes for lithium ion batteries, photocatalyst and solar energy conversion, gas sensor, field emission effect (Muhammad et al., 2020). Research in the field of copper oxides continues to uncover new and exciting properties. Their facile fabrication and use together with their abroad properties make them an ideal choice for the project.

In this study, we suggest the use of a highly sensitive, non-enzymatic metal oxide sensor based capable of determining concentrations of nitrate. The disposable nitrate sensor is based on tin doped copper oxide deposited on a fluorine dope tin oxide to generate a quantifiable amperometric response.

1.2 Problem statement

Nitrate pollutant is a major environmental problem worldwide and a public health concern requiring the development of effective and sensitive detection techniques. It has been a main concern for many researchers nowadays. It is essential to monitor the contaminating ions on a regular basis to keep the groundwater or drinking water clean and safe. Conventional detection methods frequently don't have the real-time, sensitivity, and selectivity capabilities needed for on-site monitoring. Although improving nitrate detection through the use of metal oxide-based amperometric sensors seems promising. There are still issues with optimizing sensor performance for real-world uses. This study intends to address this issue by employing a novel Sn-Cu_xO nanocomposite for amperometric nitrate detection in aqueous solutions. The following important research questions in the fabrication of metal oxide-based amperometric nitrate sensors are the focus of this study; consequently, the development of simple, highly sensitive, low cost, disposable sensors for nitrate is of most important.

1.3 Research questions

- How does the electrochemical behavior of the Sn-Cu_xO nanocomposite contribute to its effectiveness in nitrate detection?
- Is the resulting non-enzymatic Sn-Cu_xO sensor sensitive to nitrate?
- Does the sensor exhibit lower detection limit towards nitrate compared to other existing methods?

- In the presence of common interferents, how selective is the Sn-Cu_xO nanocomposite sensor for nitrate?
- What is the performance of the Sn-Cu_xO nanocomposite sensor in actual real water samples?
- What is the sensitivity, selectivity, and practicality of the Sn-CuxO nanocomposite sensor in comparison to other nitrate detection techniques?

1.4 Aim and Objectives

The main aim of this research is to fabricate a sensor that is highly sensitive to nitrate and has rapid response at lower detection limit.

The objectives of this research will be:

- To synthesis the Copper oxide nanoparticles,
- To fabricate the sensor using Tin and Copper oxide nanoparticles and perform the electrochemical testing, to gain insights into the mechanisms that underlie nitrate detection,
- To investigate and optimize the Sn-Cu_xO nanocomposite's composition in order to improve its electrochemical characteristics for nitrate detection,
- To develop electrodes with the Sn-Cu_xO nanocomposite to ensure reproducibility and stability in nitrate detection,
- To explore and optimize operational conditions such as potential scan rates to maximize the stability of the as prepared sensor,
- To evaluate the sensitivity and selectivity of the Sn-Cu_xO nanocomposite-based sensor for nitrate detection over a range of concentrations in the presence of potential interfering species commonly found in water,
- To characterize the synthesized undoped and Sn-doped Cu_xO thin films using XRD, SEM and XPS analysis,
- Use previous approved works to compare the Sn-Cu_xO nanocomposite-based sensor's performance,
- To publish the research findings through publications in scientific journals and presentations at conferences.

1.5 Importance of the research

One of the major reasons to develop a low-cost portable device is to monitor the nitrate concentration continuously in aqueous media. This research based on the electro

characterization of the as prepared sensor will be beneficial to different range of area including the environment and science field as it has not been reported before and will enhance the modern science. The results may contribute to the development of nitrate detection sensing technologies, providing an important means of ensuring the sustainability and safety of water resources.

1.6 Delineation of research

In this research, the experiments were only analyzed on a laboratory scale.

1.7 Organization of thesis

This work is subdivided into five chapters:

Chapter 1: Introduction

This chapter presents an overview of this research study subdivided in introduction, problem statement and the different research questions, the aims and objectives, the importance of the research, the delineation and the organization of the thesis.

Chapter 2: Literature review

This chapter presents the detailed theory and knowledge on the reduction of nitrate and the different methods being used. On Copper oxide and tin as catalysts, their different properties and applications. As well as the emphasis on the electrochemical analysis and different physical characterizations.

Chapter 3: Methodology

This chapter details the experimental procedure employed for the reduction of nitrate, the material and chemicals used, the instrumentation and equipment utilized. The software as well as the handling of data collection used are also presented.

Chapter 4: Experimental results and discussion

This chapter reveals all the results obtained from experiments. The analyzing and interpretation of the electrochemical characterization of the undoped and Sn-doped Cu_xO as well as their physical characterization are discussed.

Chapter 5: Conclusion and recommendations

This chapter gives a summary of the research from the introduction to the results of obtained from the experiments as well as some recommendations.

Bibliography

A summary of all the references used in this report as well as for overall knowledge.

Appendix

Summary of data and software used. As well as an extract from the published paper from this research project.

Chapter 2 : Literature Review

2.1 Introduction

This chapter gives an overview and a literature review on the reduction of nitrate using a metal oxide nanoparticles synthesized via a simple chemical route. It presents the different methods used for the detection of the particular analyte, the different supporting materials utilized as catalysts. In this project Sn-Cu_xO, as well as the characterization techniques are discussed in depth in this section.

2.2 Nitrate Overview

Nitrate is a chemical species composed of nitrogen and oxygen compounds naturally found into the environment and the water systems such as groundwater. It comes from many sources, the major includes agricultural activities where it is extensively used as fertilizers, from landfilling, animal wastes, septic and sewage system as well as industrial wastewater treatment system (Suresh et al., 2019). Nitrate has positive effects on health such as the oxygen intake, the protective effects on the cardiovascular system, it plays an important role in the regulation of blood pressure and the improvement of blood flow through biological conversion to nitrite and nitric oxide and secondary reaction products, such as nitrous, nitrile (Lundberg et al., 2006). Studies have shown that nitrate can be found naturally in breast milk where it acts as an important nutritious element in the protection of the baby (Hord et al., 2011). Nitrates are also used as preservatives to stabilize color, create fragrance and control food spoilage. they also inhibit the growth of other microorganisms (Sindelar and Milkowski, 2012).

2.3 Sources of human exposure and negatives effects of Nitrate

Despite the many positives effects of nitrate in the human life and the environment, nitrates are harmful to human and aquatic life when exposed to high concentration. Their high solubility in water facilitate their transportation throughout the water systems and therefore facilitating the contamination (Sohail and Adeloju, 2016). Nitrogen compounds such as nitrates are required to support production in aquatic ecosystems, but the increase in their concentration can therefore increases the growth and production leading to the phenomena of eutrophication (Gutiérrez et al., 2018). The latter is generally referred to as the biological effects of high concentrations of nutrients such as N-compound and P-compound on ecosystems.

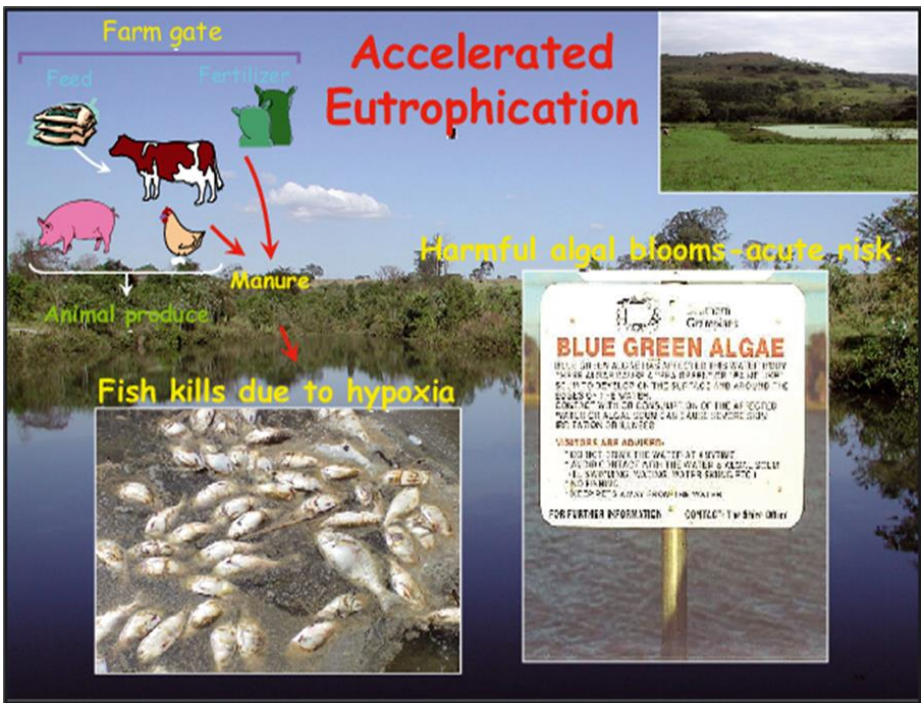

Figure 2.1: Effect of Nitrates

(Sigua, 2011)

The cause of the increase in nitrate concentration in surface water and groundwater comes from the pollution of human, animal and agricultural waste as well as the leachate from the waste pile. Others sources of contamination includes food, air and soil. Serious health hazards have been associated with consumption of water with high nitrate concentrations. The phenomena of toxicity in the human body occurs generally when the nitrates in excess are reduced to nitrites converting the hemoglobin to methemoglobin which in turn interfere with the transportation of oxygen in the blood (Stortini et al., 2015), causing what is called Methemoglobinemia or blue baby syndrome (oxygen deficiency). The symptoms generally encountered may include shortness of breath and skin blueness. The other mechanism of nitrate conversion into nitrite in the human body generate a chain in the stomach with amines and amides forming N–nitrosamines, a carcinogenic compounds causing gastric cancer. The relative standard has been established by various organizations to limit the concentration of nitrate in food and drinking water because of the damages held by their higher concentration. The World Health Organization (WHO) (WHO, 2011) set the safe limit of nitrate in potable water to be 50 mg NO_3^-/L (WHO, 2011), Whereas Italian regulations reported it to be 45 mg NO_3^-/L and 10 mg NO_3^-/L for infants while the United States Environmental Protection Agency (EPA) recommends 44.2 mg NO_3^-/L (Amali et al., 2021).

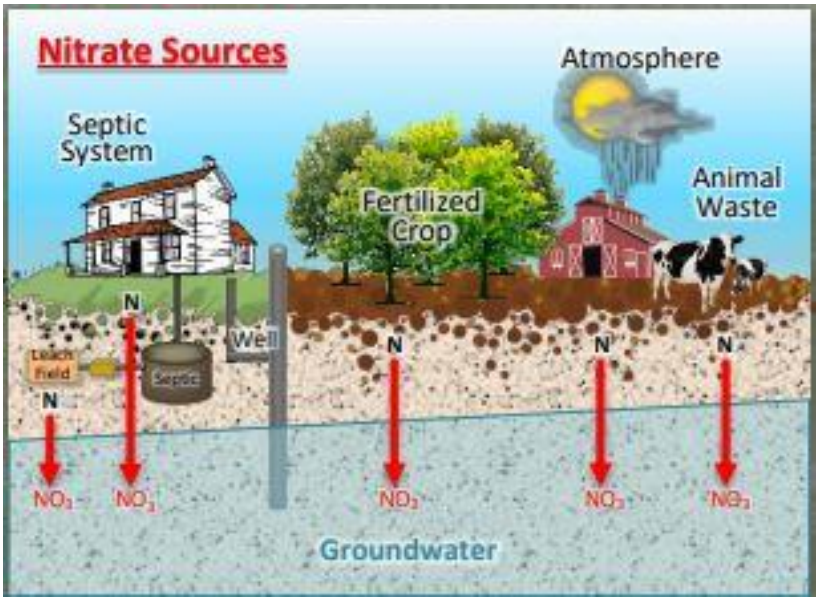

Figure 2.2: Sources of Nitrate pollution

(Stevenson, 2019)

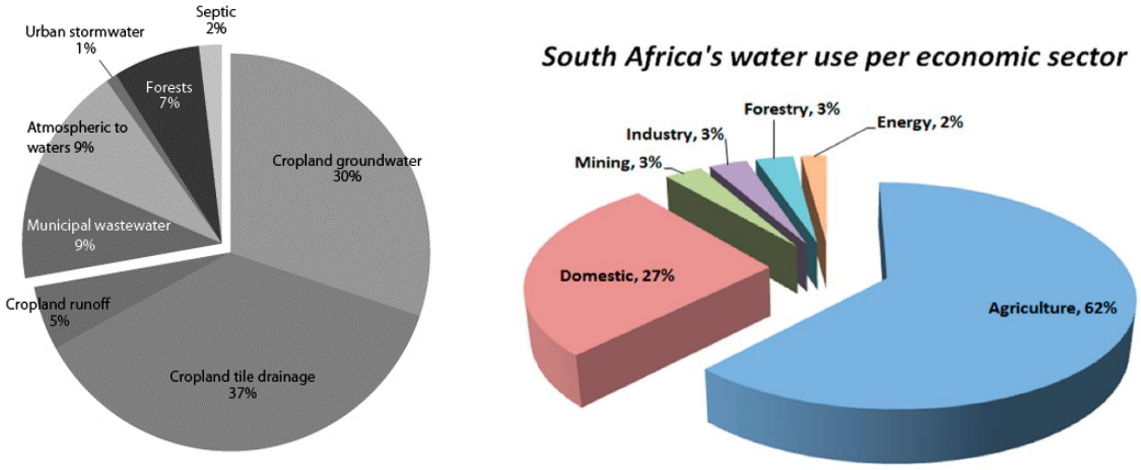

Figure 2.3: Statistic of Nitrate pollution per area

(Askham and Van der Poll, 2017)

2.4 Nitrate detection methods

Many sophisticated techniques have been used for the efficient detection of nitrate, which includes ion-chromatography (Fu et al., 2015), spectroscopic method (Jahn et al., 2006), chemiluminescence (Kodamatani et al., 2009), Raman spectroscopy (Kim et al., 2012) etc. However, these methods have drawbacks such as complicated working steps, interferences and the high cost and sophisticated instrumentations that are required to perform the analysis. On the other hand, electrochemical technique is a more efficient and promising high performance tool with an excellent advantage of reliability, high sensitivity, short response time, good selectivity, easy simple set up and cost effective in sensing nitrate ions in comparison with the previous mentioned techniques (Siddiqui et al., 2021).

Table 2.1: Comparison of different conventional methods (Alahi and Mukhopadhyay, 2018)

Method	Feasibility	Complexity	Sensitivity	Cost	Interferences
Chromatography	Requires multiples steps	Requires expensive equipment and complex reagents	High	High	Ions with similar retention time
Colorimetry	Require multiples steps	Needs few equipment, low complexity	Poor	Low	ions
UV-Vis spectroscopy	Requires sample to be collected	Needs optic, medium complexity	High	Medium	Organic components and ions
Electrochemistry	Easily performed	Low complexity	Medium	Low	Complex sample

2.4.1 Electrochemical methods

Electrochemical technique consists of converting the response obtained between the interaction of the analyte and the sensing component using an electrochemical sensor into a measurable signal corresponding to the concentration of the analyte in a particular matrices (Alahi and Mukhopadhyay, 2018). It utilizes an electrochemical cell consisting of a three electrode system; the counter electrode (CE), the working electrode (WE) and the reference electrode (RE) (Figure 2.4). The CE also refers to as the auxiliary electrode (AE), provides a means of applying an input potential to the WE; it completes the circuit and allow the flow of electrons. WE is where the electron transfer occurs and it is modified to enhance the electro

catalytic reaction of the sensor using different nanomaterials. Whereas RE ensures and controls the WE potential (Alahi and Mukhopadhyay, 2018). Different electrochemical methods have been employed in the reduction of nitrate sensors depending on the interactions interface between nitrate and the material used. Recently, many studies have been devoted to the development of voltammetric, amperometric, potentiometric and electrochemical impedance spectroscopy (EIS) methods of analysis. The latter being less employed in the sensing application.

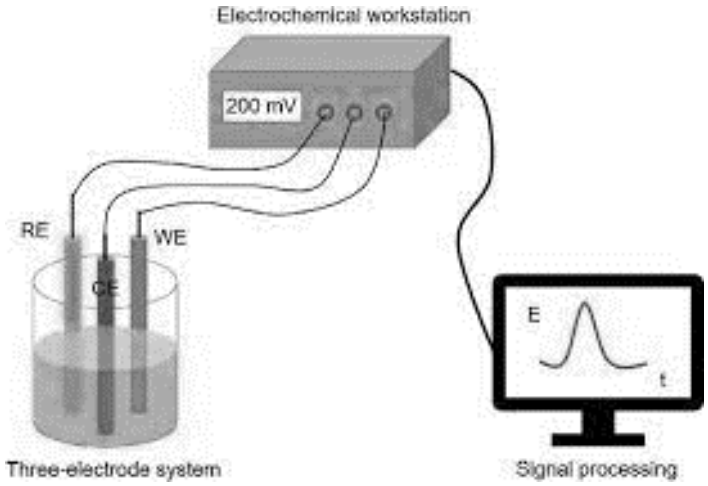

Figure 2.4: Electrochemical cell representation

(Bansod et al., 2017)

2.4.2 Voltammetric techniques

Cyclic voltammetry (CV), linear sweep voltammetry (LSV), differential pulse voltammetry (DPV) and square voltammetry (SWV) are the most employed voltammetric techniques in sensing for nitrate detection. These methods differ in the way the potential is varied. CV is one of the common effective techniques used in the nitrate sensing application to obtain useful information on the redox behavior (oxidation/reduction) modification processes of the electrodes and to understand the mechanisms and kinetic parameters involved in the reactions. As the name indicates, cyclic voltammetry is based on varying the applied voltage of the WE in both the forward (anodic) and the reverse (cathodic) reactions while the current

generated by the electrochemical reaction is being measured (Figure 2.5) (Heydari et al., 2016).

Gumpu et al. (2017) reported a voltammetric method based on cyclic voltammetry to determine the nitrate concentration in water. Zinc oxide was electrochemically deposited on the platinum electrode which was serving as the working electrode. The linear response concentration range was from 0.1 mM to 2 mM with a low detection limit and high sensitivity of 10 nM and 39.91 μA/cm2 mM, respectively.

Amertharaj et al. (2014) reported a voltammetric determination of nitrate using a platinum-copper electrode in alkaline medium.

Li et al. (2022) demonstrated a novel Copper/Carbon nanofibers/carbon fibre microelectrode (Cu/CNFs/CFE). It has shown an increased sensitivity and a lower limit of detection for nitrate of 0.8 μM (S/N = 3) and a linear range from 5 μM–8000 μM.

LSV is one of the simplest voltammetric methods, with the current being measured linearly with an increase in the applied voltage over time. DPV and SWV utilized pulse techniques on a potential staircase. The difference between them is that in SWV, the currents difference are measured between the forward and reverse pulse currents, while in DPV the current is measured right before and after each pulse is applied (Stortini et al., 2015).

A differential pulse voltammetric method based on a copper-plated glassy carbon was applied to determine the nitrate in natural water. The detection limit was found to be 2.8 μM, the linear detection range was from 2.8 μM up to 80 μM and the sensitivity of 968.3 mA L/mole (Ramakrishnappa et al., 2020).

Amali et al. (2021) reported a similar copper plated glassy carbon electrodes for the determination of nitrate using the square wave voltammetric method. The linear range was 0.61 μM- to 50 μM and the LOD was 0.18 μM.

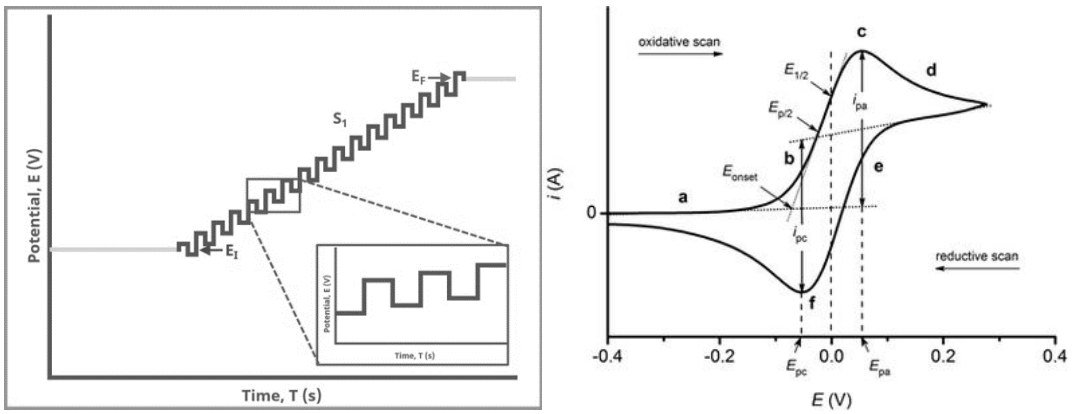

Figure 2.5: Square wave voltammetry and Cyclic Voltammetry graphs

(Simões and Xavier, 2017, Climent and Feliu, 2018)

2.4.3 Amperometric methods

Amperometric method is an effective technique of measuring the current as a function of time at a constant voltage driving the reduction of nitrate. It is very simple to perform. Amperometric sensors have been attributed the merit of achieving high sensitivity, selectivity and low detection limits for nitrate reduction (Bommireddy and Palathedath, 2020). The study to estimate the amount of the electroactive species is done through a current plot (I-t) referred to as the voltammogram (figure 2.6) using the generated current obtained during the measurement. The highest peak is normally an indication of the highest amount of current generated. The concentration of the analyte is typically determined by choosing a time t_t between the points long after the initial time t_o so that the current at that time will be proportional to the concentration of the analyte (Felix et al., 2018).

An amperometric method to determine the nitrate in water was reported by Carpenter and Pletcher (1995) with a concentration range of up to 1 mM Polypyrrole (PPy)-nanowire modified electrodes based on graphite electrodes were reported for nitrate detection (Bommireddy and Palathedath, 2020). The detection limit was 1.52 µM and the sensitivity was 336.28 mA/M cm^2.

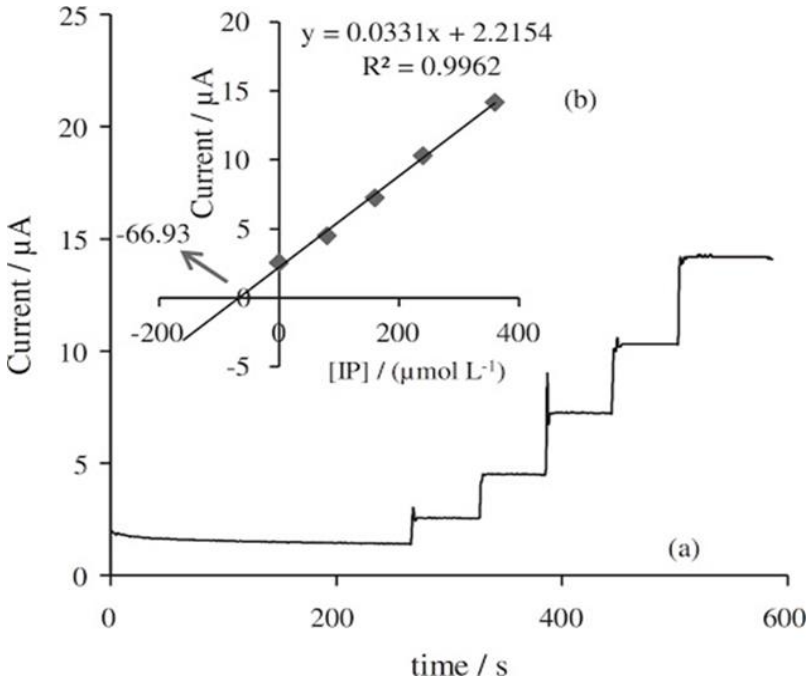

Figure 2.6: Current vs Time amperometric graph

(Žabčíková et al., 2016)

2.4.4 Potentiometric methods

Potentiometry is a technique at zero current meaning that the potentials are measured while there is no current flowing. Typically, potentiometric devices measure the potential difference between the RE and an ion selective electrode in the absence of current (Gil et al., 2019).

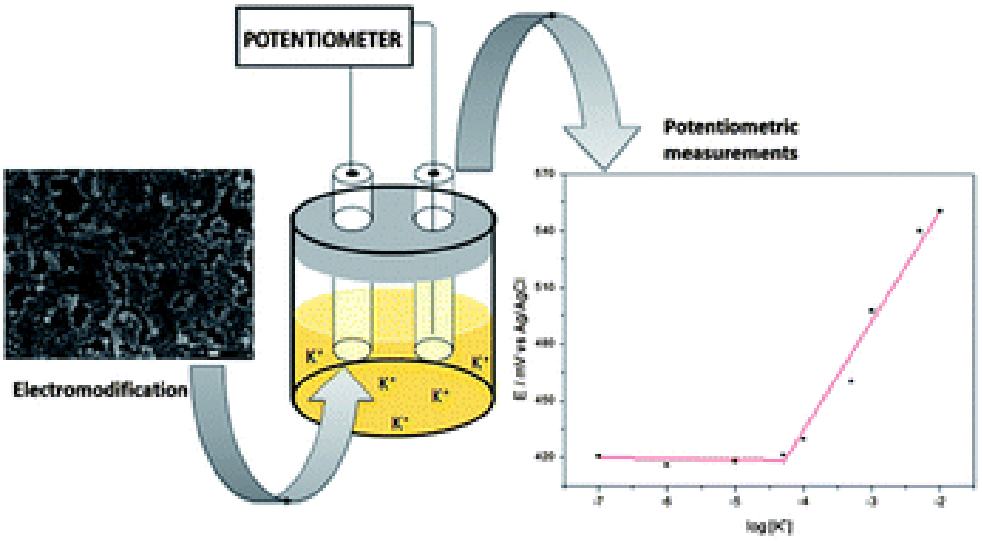

Figure 2.7: Potentiometry

(Sedenho et al., 2013)

2.4.5 Electrochemical impedance spectroscopy methods

EIS is a technique of analyzing the charge transfer resistance of the surface of the electrode. It is a method to determine the current response of an electrochemical cell by applying a small sinusoidal signal. It is widely used in various fields. A periodic sinusoidal voltage is applied to the sensor, creating a phase shift between the applied voltage and current flow through the sensor, implying that the total impedance is composed of two parts: the real part and the imaginary part. Two most important representation methods that show the specific parameters are the Nyquist plot which represents the relationship between the real part of impedance and the imaginary part in a particular frequency range and the bode plot illustrating the frequency absolute impedance (Z) and phase angle (θ) (Esser et al., 2022).

The Randles equivalent circuit is used to express EIS representation in electrical model form. It consist of a series of resistance R_e, Capacitance C_{dl}. Charge transfer impedance Z_w and charge transfer resistance R_t as shown in figure 2.7.

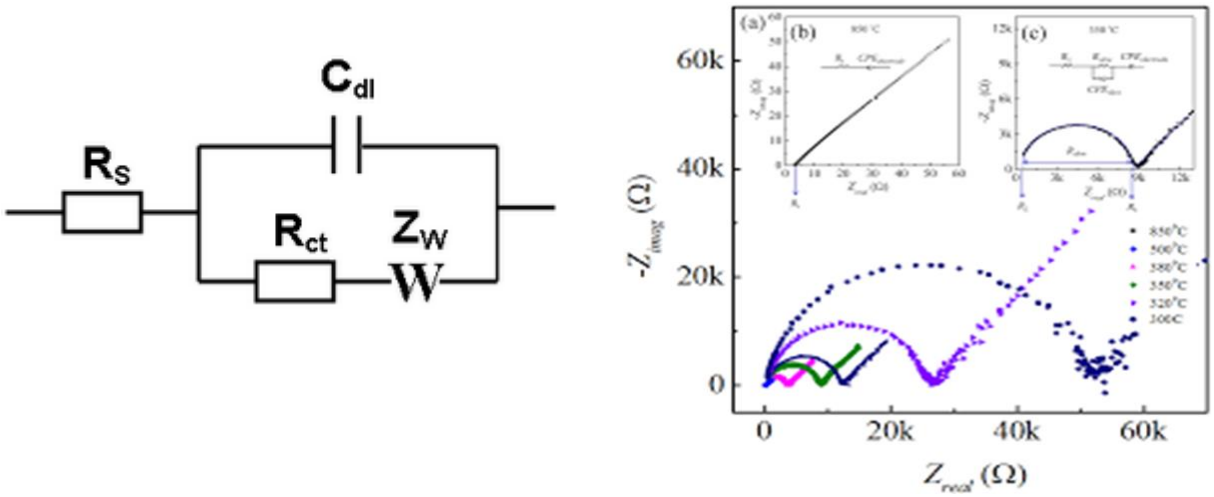

Figure 2.8: Randles equivalent circuit and Nyquist plot

(Hammouda and Kamel, 2020)

2.5 Sensors for detection of nitrate

Electrochemical sensors are devices containing an electrochemical transducer, which can convert the response obtained by the interaction between the target analyte and the sensing element into a measurable signal corresponding to the concentration of the analyte (Adlakha-Hutcheon et al., 2009).

Non-enzymatic nitrate sensors based on conductive polymers, graphene and graphene oxide, carbon nanotubes and fibers, metals, and bimetals have been extensively explored in contrast to transition metal oxides (Amali et al., 2021).

Over the years, most frequently used electrodes including mercury, glassy carbon, platinum and gold were reported to have difficulty in the reduction of nitrate. However, the use of modification surfaces of the solids electrodes materials are reported to enhance the electro activity of nitrate ions reduction. Several nitrates sensors have been studied that include Copper (Aouina et al., 2010), Cobalt (Amali et al., 2021), Iron (Wang et al., 2017), Ag (Fajerwerg et al., 2010), bimetallic electrodes (Amertharaj et al., 2014), boron doped diamond (Kuang et al., 2018) etc. Copper is one among other material that have been extensively used sensor development. It is known to have great stability and great electrochemical properties.

2.6 Metal Oxides

Compared to others non enzymatic sensors, metal oxides have not yet been studied extensively. However, previous studies on the latter reported their good catalytic properties and their improvement in the electron transfer processes associated with the detection of different analytes (Amali et al., 2021). Among those metals oxides, Copper oxide is the focus of interest due to its low cost, ease of preparation, high synergistic stability and catalytic activity as well as the rapid electron transfer kinetics (Aazadfar et al., 2018). Copper oxide have multiple oxidation states which also promote the redox reactions. At the same time, oxygen vacancies are deemed to favor adsorption and facilitate dissociation of oxygen-containing species or their electro catalytic reduction (Balık et al., 2019). The (110) crystal plane of CuO has been found to be propitious to excellent catalytic performance due to its higher surface energy than those of the (111) and (-111) facets (Balık et al., 2019).

2.6.1 Fundamental Properties of Cu_xO

Copper oxide (Cu_2O and CuO) is a material with interesting characteristics. Material containing both Cu_2O and CuO phases are referred as mixed copper oxide. Researchers often look into ways to modify the properties of mixed copper oxide materials by adjusting for instance the composition, crystal structure, or introducing additional elements (doping) into the structure. For example, by adding others elements such as Sn in the case of Sn-Cu_xO nanocomposites in this study. This tuning can improve certain characteristics for targeted applications. Cu_xO crystal has monoclinic structure & cubic structure (Figure 2.9 & 2.10 respectively) and belongs to symmetry. Cupric oxide has four formula units per unit cell. The coordination number of copper atom is 4, which means that it is linked to four oxygen neighbor atoms in an approximately square planar configuration in the (110) plane. In all crystallized solids, divalent copper surroundings are always very distorted by a strong Jahn-Teller effect which often leads to more stable square planar groups. Furthermore, possible oxidation states are Cu^+, Cu^{2+} and Cu^{3+}, Thus CuO allows both electron and hole doping (Baturay et al., 2019). The stability and behavior of the electrochemical process can be influenced by the combination of different copper oxide phases. When compared to single phases, mixed copper oxide materials can have higher catalytic activity because of the synergistic effects of CuO and Cu_2O. Their coexistence allows for controlled redox chemistry. This can be beneficial in applications where controlled oxidation and reduction reactions are required, such as in electrochemical sensors in this case.

Ramakrishnappa et al. (2020) reported a copper oxide (Cu_xO) impregnated glassy carbon spheres (Cu_xOGCS) modified basal plane pyrolytic graphite electrode as an electrochemical sensor for nitrate detection. The detection limit obtained was 1.032 µg/L for nitrate. The sensitivity was about 1, 5 µA mM^{-1} cm^{-2}.

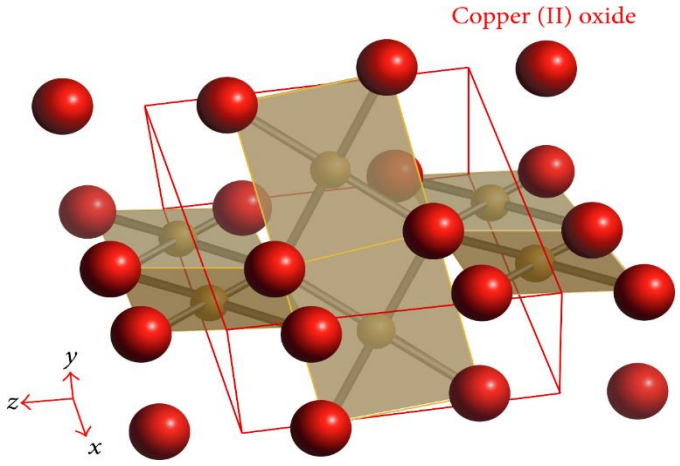

Figure 2.9: CuO structure

(Shang and Guo, 2015)

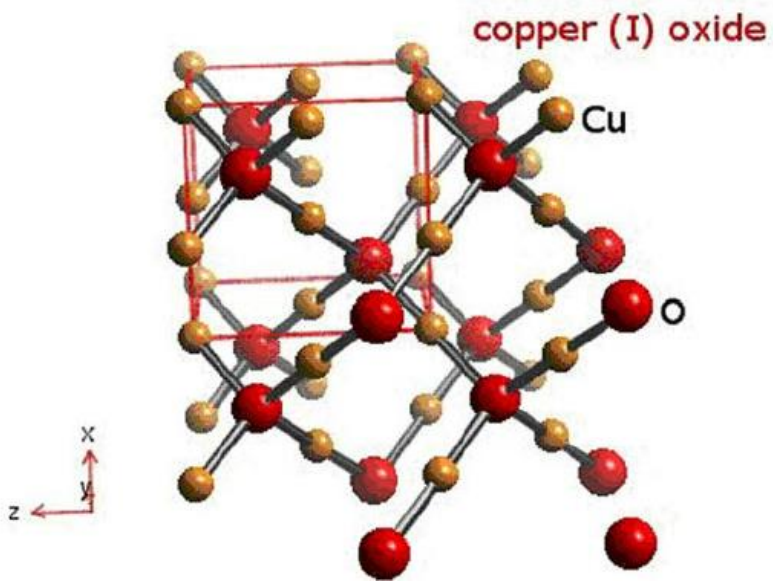

Figure 2.10: Cu_2O Structure

(Petrovic et al., 2011)

In this study, a facile and quick synthesis of metal organic decomposition undoped and Sn-doped copper oxide composite thin films by spin-coating deposition on the Fluorine tin oxide substrate for the detection of nitrate in basic medium was reported for the first time. The influence of Sn doping on the physicochemical and electrochemical properties of Cu_xO thin film for nitrate detection was further discussed. Such study has not yet been conducted. Previous researchers have solely focused on the characterization and practical application of Sn-doped Cu_xO (Mohebbi et al., 2013).

2.7 Depositions method (depositing monolayers & thin films of nanoparticles)

There are numerous techniques to deposit monolayers and thin films of nanoparticles onto a substrate. The choice of technique to obtain the desired morphology and thickness depends on parameters such as the available equipment, the area to be covered on the substrate, the choice of solvent, temperature, and particle concentration, etc.

Here are some of the techniques used; Drop casting, spray coating, spin coating, electrodeposition, dip coating, substrate/particle surface functionalization etc. The method of preference used in this work is spin coating.

2.7.1 Spin-Coating

Spin coating method is a technique in which the substrate is spun at high RPM and a particular volume of the solution deposition with a known concentration is spread over the area to be covered at the center. The mechanism uses centrifugal force that leads to uniform spreading of the solution across the area of the substrate, followed by evaporation of the solvent to obtain a thin film. Spin coating often provides a more uniform thickness across the substrate but that depends on the solution concentration, volume and the speed velocity utilized (Larson and Rehg, 1997). Fluorine-tin-doped glass substrate is used as the support of Sn and Cu particles instead of the most commonly used glassy carbon as it is cheaper and available.

2.8 Characterizations techniques

The characterization of a solid surface depends enormously on the chemical structure of the surface. Analyzing a surface simply means studying the chemical structure of an extremely thin area. Light, x-rays, and electrons are used for surface study and stimulation.

2.8.1 Electron Microscopy

Electron microscopy is a technique use to obtain high resolution images in different fields including science, technology, forensics, etc. to provide useful information on the structure being studied. There are two most common types of electron microscopy namely scanning electron microscopy (SEM) and transmission electron microscopy (TEM).

2.8.1.1 SEM

Scanning electron microscopy (SEM) is a type of electron microscopy technique that is employed to produce a visual image of a sample surface scanned by a high energy electron beam (figure 2.11). The sample interacts with the electrons and provides information about the morphology, topography, composition, chemistry, etc. Morphology gives details about the shape and size while topography gives an overview on the surface features of a sample, e.g. the texture or roughness. Composition indicates the elements and compounds found in the material (Bin Mobarak et al., 2022).

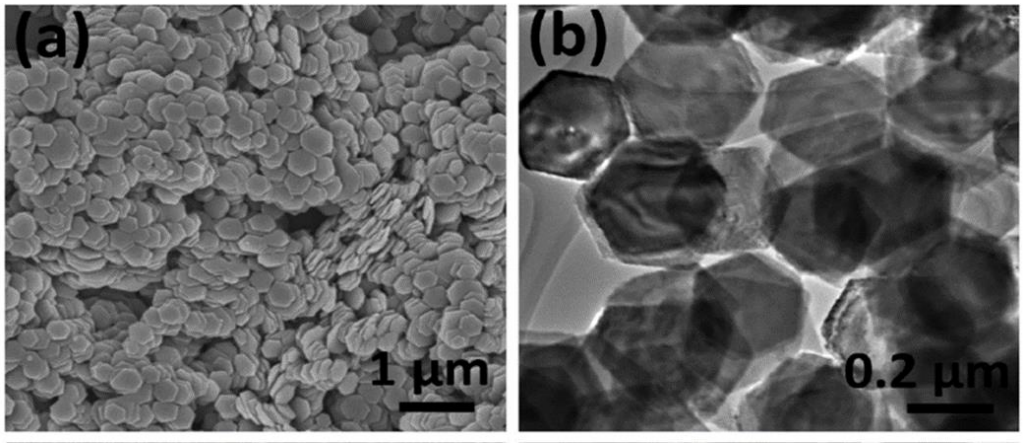

Figure 2.11: SEM images representation of metal oxides nanostructures

(Thiagarajan et al., 2017)

2.8.1.2 TEM

Transmission electron microscopy (TEM) is an electron microscopy technique that provides information on the internal structure of a sample image using a beam of electrons. The electron beam that passes through produces an image with details on the morphology, composition and crystal structure (Bin Mobarak et al., 2022).

2.8.1.3 XRD

X-ray diffraction analysis (XRD) is a common technique used to determine the crystallographic structure of a material as well as the purity of the product (figure 2.12). It is also used to determine the structural properties such as Lattice parameters, Strain, Grain size, Epitaxy, Phase composition, preferred orientation, Measure thickness of thin films and multi-layers, Determine atomic arrangement. XRD works by exposing a material with incident X-rays (Abuelwafa et al., 2021). Elastic scattering is happening, Crystal atoms scatter incident X-rays through interaction with the atoms' electrons; the latter is called the scatterer. The intensities and scattering angles of the X-rays that leave the material are measured. These scatterers produce a regular array of spherical waves where their interference cancel each other however according to Bragg's law, they constructively add to each other (Yang and Zhao, 2008).

$$2d\sin\theta = n\lambda \quad (1)$$

Where *d* is the spacing between diffracting planes,

θ is the incident angle,

n is an integer, and

λ is the beam wavelength.

X-rays are used to produce the diffraction pattern because their wavelength, λ, is often the same order of magnitude as the spacing, *d*, between the crystal planes (1-100 angstroms).

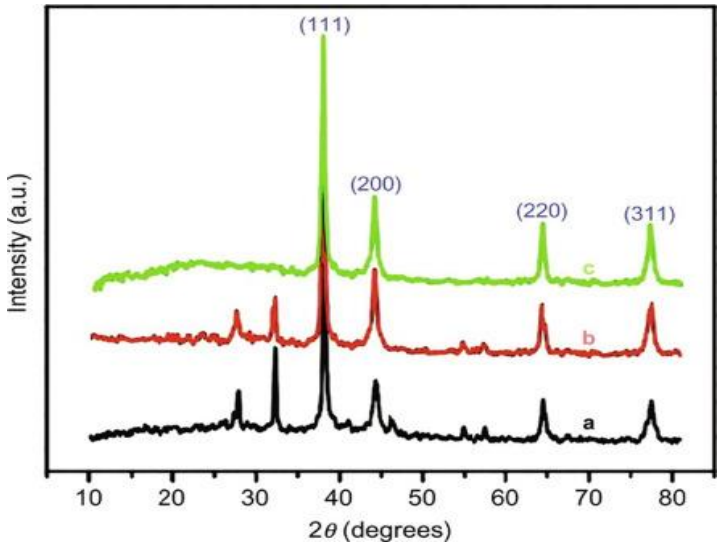

Figure 2.12: XRD pattern of silver nanomaterial

(Raja et al., 2022)

2.8.1.4 XPS

X-ray Photoelectron Spectroscopy (XPS) is a technique in which a sample surface is irradiated by X-rays to analyze the elements constituting the surface of the sample, its composition, and chemical bonding state and also analyze the kinetic energy of the photoelectrons generated from the sample surface (figure 2.13) (Ciftyürek et al., 2019).

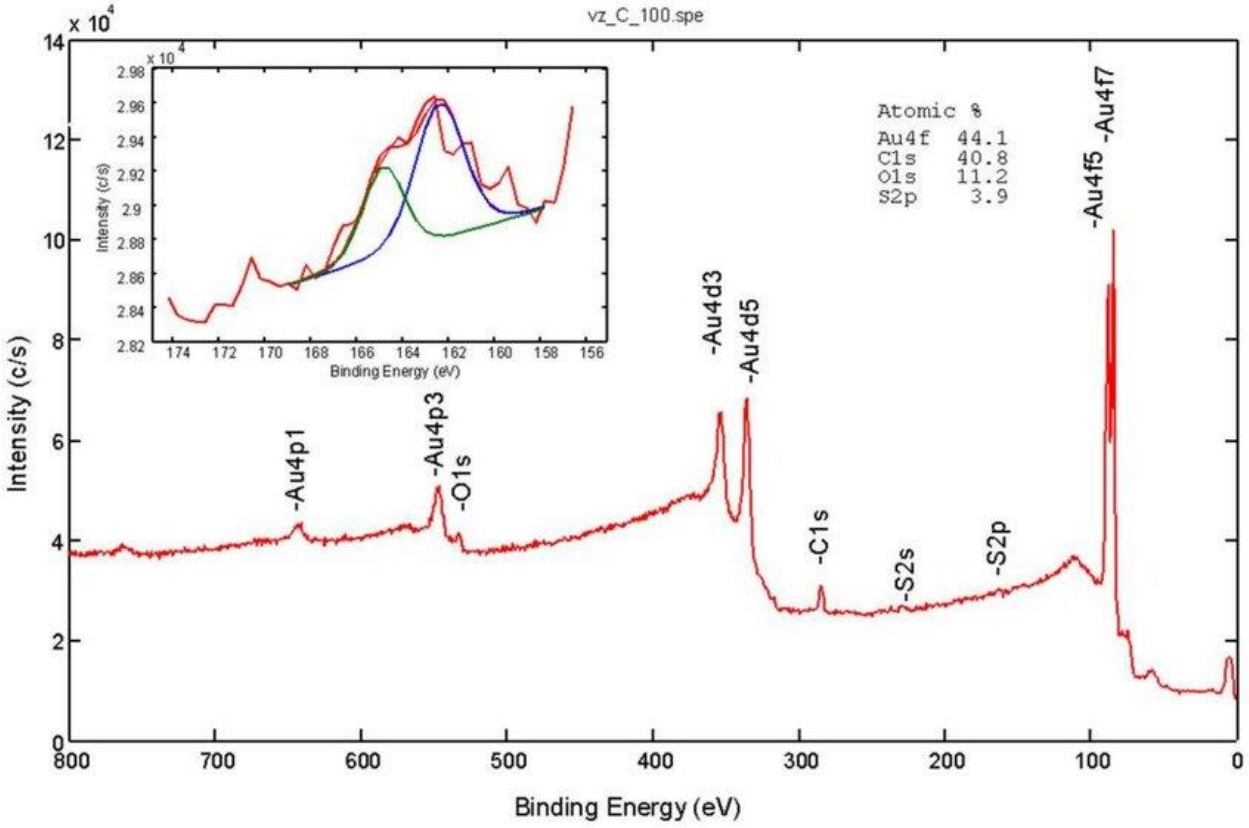

Figure 2.13: XPS technique

(Strle et al., 2014)

2.9 Mechanisms for nitrate reduction

It is important to understand the mechanism of nitrate reduction to better explain the electrochemical behavior of the material used. The mechanism of the electrochemical reduction of nitrate in non-enzymatic sensors leads to a complex electron transfer process, resulting in the formation of nitrite as the rate-determining step, with the latter being reduced to other N-compounds, namely ammonia or nitrogen gas as described in the equations below (2-14). In order to obtain the intermediates and end products demonstrated in equations (2-4), some factors are to be considered that includes the material used to modify the surface of the electrode, the electrolyte used, the pH of the medium, and so on (Alahi and Mukhopadhyay, 2018). The reduction of nitrate occurs at more negative potentials than thermodynamic values indicating an over potential and an high activation energy confirmed by the slow reaction kinetics in equation 2 (Toktarev and Echevskii, 2008). Normally, the reduction of nitrate happens with the adsorption of ions from the solution onto the electrode surface, mass transfer is observed and therefore concentration of nitrate is involved thus limiting the adsorption process and the entire process of the electrochemical nitrate reduction. Consequently,

concentration of nitrate is important because it defines the diffusion rate between the electrolyte and the electrode and according to Fick's law, the rate of diffusion of a substance is proportional to the concentration gradient of the particle (Mauro, 2021).

Fajerwerg et al. (2010) demonstrated the adsorption of nitrate on the surface of Au electrodes that occurs in a two-step coordination where nitrate donates two pairs of electrons to the Au atom. The free sites on the surface of the electrode must be in correlation with the oxygen to activate the transition state leading to the breaking of the N-O bond in the reduction of nitrate.

According to Suresh et al. (2019), following are the intermediate steps in the reduction of nitrate. The first initial reduction yields a short lived of about 20 μs nitrate di-anion radical (NO_3^{2-}) by reaction (2) (Tyagi et al., 2018). The next reaction is the chemical reaction consisting of the hydrolysis of NO_3^{2-} leading to nitrogen dioxide radical (NO_2) in reaction (3) (Amali et al., 2021). Continually, in reaction (4), NO_2 is further reduced via the second charge transfer reaction route to NO^{2-}. Furthermore, as shown by reactions (5-14), Electrochemical reduction to nitrite, is considered as the electro reduction limiting step for the overall reduction mechanism of nitrate to ammonia and nitrogen gas.

$NO_3^- + e^- \rightarrow NO_3^{2-}$ (2)

$NO_3^{2-} + H_2O \rightarrow NO_2 + 2\ OH^-$ (3)

$NO_2 + e^- \rightarrow NO_2^- + H_2O$ (4)

$E^o = -0.89$ V vs SHE $k = 5.5 \times 104\ s\text{-}1$ $E^o = 1.04$ V vs SHE

A summary of the general reactions that can occur during the electro catalytic reduction of nitrate is given by

In acidic medium

$NO_3^- + 2\ H^+ + 2\ e^- \rightarrow NO_2^- + H_2O$ $E^o = 0.01$ V vs SHE (5)

$NO_3^- + 2H^+ + 2e^- \rightarrow NO_2^- + H_2O$ (6)

$NO_2^- + 8H^+ + 6e^- \rightarrow NH_4^+ + 2H_2O$ (7)

NO_3^-+ 10H^++ 8e^- → NH_4^++ 3H_2O (8)

In neutral or alkaline medium

NO_3^-+H_2O + 2e^- →NO_2^-+ 2OH^- (9)

NO_2^-+ 5H_2O + 6e^- →NH_3+ 7OH^- (10)

NO_2^- + 4H_2O + 4e^- →NH_2OH + 5OH^- (11)

NH_2OH +H_2O + 2e^- →NH_3 + 2OH^- (12)

2NO_2^-+ 3H_2O + 4e^- → N_2O + 6OH^- (13)

2NO_2^-+ 4H_2O + 6e^- → N_2+ 8OH^- (14) (Jasna et al., 2020)

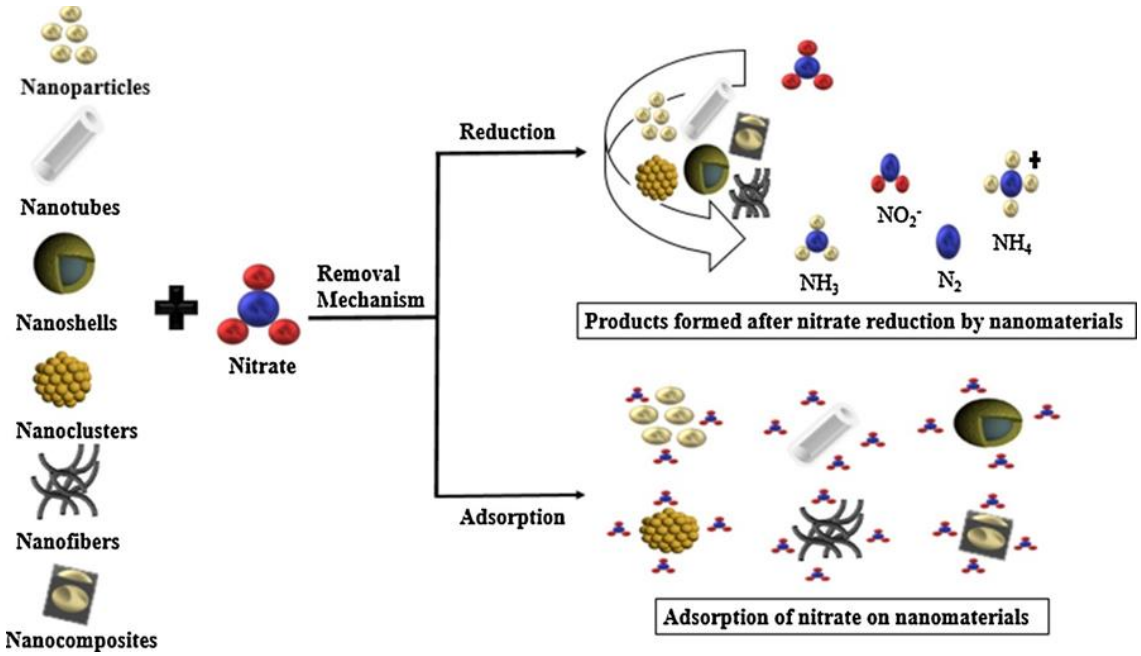

Figure 2.14: Mechanism of nitrate removal

(Tyagi et al., 2018)

2.10 Conclusion

Nitrate as a chemical compound composed of nitrogen and oxygen, naturally present in the environment and water systems like groundwater. It originates from various sources, primarily agricultural activities, landfilling, animal waste, septic and sewage systems, and industrial wastewater treatment. It can be harmful when present in high concentrations.

This section provides an overview of a research project focused on the reduction of nitrate using metal oxide nanoparticles synthesized through a chemical route. The chapter includes a literature review, the significance of nitrate, sources of exposure, detection methods, and a detailed explanation of electrochemical techniques, for nitrate detection. The text delves into various metal oxide materials, with a specific focus on Copper oxide (Cu_2O and CuO), and introduces the novel aspect of Sn-doped copper oxide composite thin films for nitrate detection. The deposition method employed is spin coating, and the chapter concludes with a comprehensive discussion of characterization techniques such as electron microscopy, X-ray diffraction, and X-ray photoelectron spectroscopy. The mechanisms for nitrate reduction, including electrochemical pathways, are also elucidated.

Chapter 3 : Methodology

3.1 Introduction

In this chapter, an outline of the research methods and techniques that were followed in this study are presented. It provides information on the materials, the procedures and the instrument that were used for data collection as well as the methods used to analyze the data.

3.2 Experimental

3.2.1 Materials

All chemicals were purchased from Sigma Aldrich South Africa and used as received without further purification. All reagents used were of analytical grade. The chemicals used to conduct this research were Sodium nitrate ($NaNO_3$), copper (II) chloride dihydrate ($CuCl_2.2H_2O$), sodium oleate ($C_{18}H_{33}NaO_2$), hexane (C_6H_{14}), ethanol (C_2H_5OH), Potassium chloride (KCl), toluene ($C_6H_5CH_3$), Potassium hydroxide pellets (KOH), Sodium hydroxide pellets (NaOH), and Tin (II) Chloride dihydrate ($SnCl_2.2H_2O$). Deionized water was used throughout the experiment. Potassium hydroxide (KOH) with a concentration of 0.1 M was used as electrolyte.

3.2.2 Electrode fabrication

The synthesis of copper oleate was done as per the procedure described by Wang and co-workers (Wang et al., 2010). Typically, 3.409 g of copper chloride dihydrate and 18.27 g of sodium oleate were dissolved in a mixture of 30 ml of water, 40 ml ethanol and 70 ml hexane resulting in a copper oleate complex. The FTO glasses were cut (4cm x 1cm) and cleaned using detergent in ultrasonic bath for 10 mins. The glass substrates were further cleaned in ultrasonic bath using ethanol and water successively for 10 min and then dried overnight in an oven at 60 ^oC. A solution deposition process was used in the production of undoped and Sn-doped Cu_xO thin films nanocomposite onto the FTO glass slide by a two-step spin coating method. 0.18 g of the resulting copper oleate complex was dispersed in 1mL of toluene in a vial and sonicated at 45 kHz for 30 to 45 mins until the solution had completely dissolved and become homogeneous to form the copper oleate complex. 0.02 g of tin chloride dihydrate was also dispersed in 0.5 ml of ETOH then sonicated for 10 min. Thereafter, 50 μL aliquot of the homogeneous copper oleate solution and 50 μL of the copper oleate and tin chloride dihydrate mixture (80:20 % v/v) were spin coated each on 1 cm^2 of a pre-cleaned and cut-to-size FTO slide at 2500 rpm for 10 s then 4000 rpm for 50 s to achieve even spreading of the thin film (the spin-coating time was decreased in this study compared to previously. In order to control

the electrode area (1 cm × 1 cm), the FTO substrate was covered partly with a tape. After spin coating, the piece of tape was removed from FTO surface. The spin-coated liquid thin films were calcined subsequently at 350 ºC for 10 min. These deposition processes were repeated four times to achieve the optimal thin film thickness of four layers with best electrochemical characteristics. The electrodes were cooled to room temperature and vacuum sealed for experimental analysis. The prepared electrodes were labelled as Cu_xO (undoped) and Sn-Cu_xO (Sn-doped).

The formation mechanism of Cu_xO thin film was proposed as: (1) decarboxylation of the oleate ligands with the release of two electrons (Chandrasekaran, 2013) (Equation 2); (2) complete reduction of cupric ion to metallic copper by the released electrons (Equation 3); (3) complete oxidation of metallic Cu species to cuprous oxide (Equation 4); (4) finally, partial oxidation of cuprous oxide to cupric oxide (Equation 5). The stoichiometric ratios of the final reaction step were deduced from XPS analysis.

$$Cu(C_{18}H_{33}O_2)_2 \leftrightarrow Cu^{2+} + 2C_{17}H_{33}COO^- \quad (1)$$

$$2C_{17}H_{33}COO^- \xrightarrow[\Delta]{} 2C_{17}H_{13}^{\bullet} + 2CO_2 + 2e^- \quad (2)$$

$$Cu^{2+} + 2e^- \rightarrow Cu \quad (3)$$

$$2Cu + \frac{1}{2}O_2 \rightarrow Cu_2O \quad (4)$$

$$3Cu_2O + \frac{1}{2}O_2 \rightarrow 2Cu_2O + 2CuO \quad (5)$$

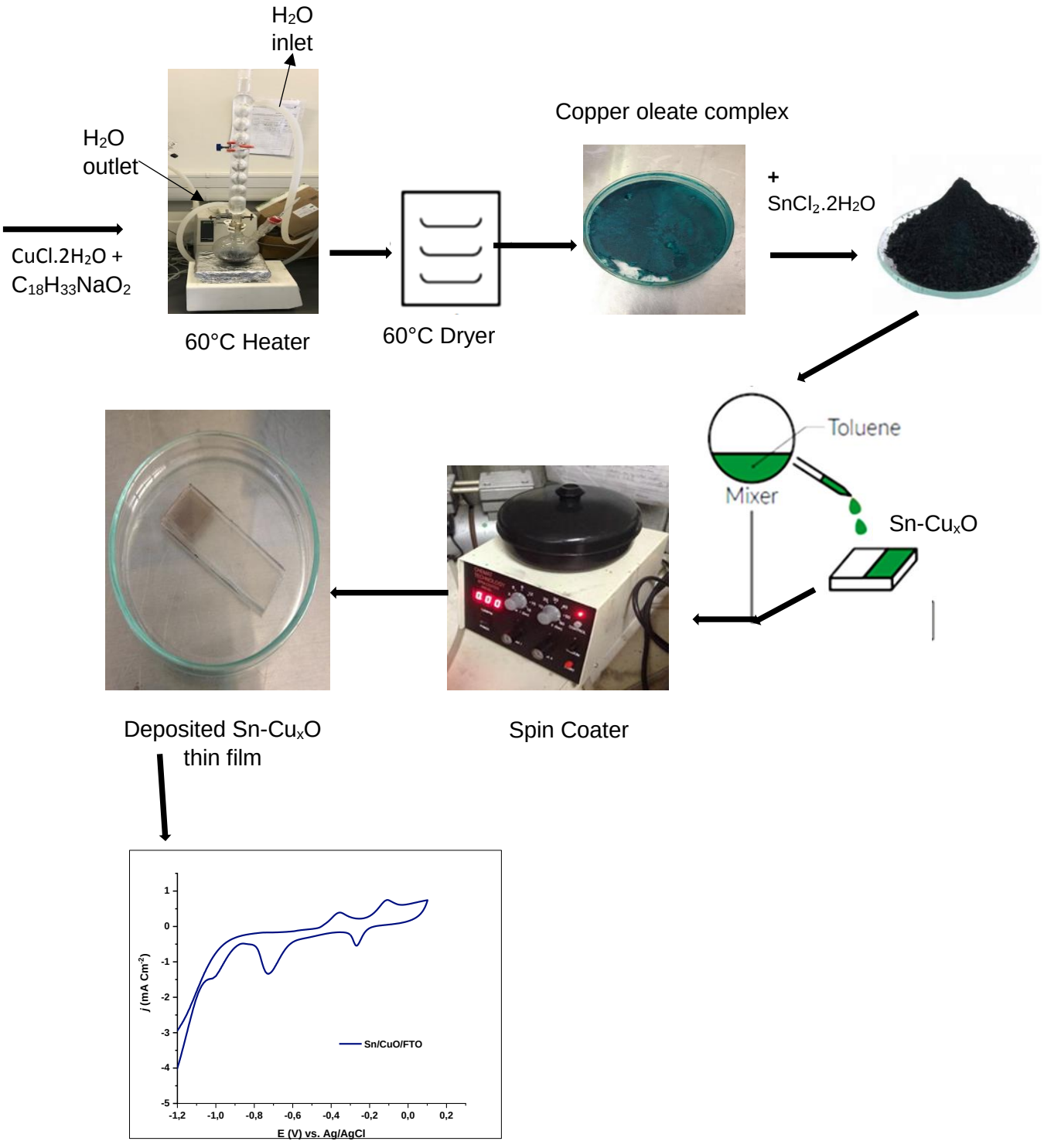

Figure 3.1: Methodology

3.2.3 Real Samples Preparation

Water samples were used for environmental sample testing. The Bore hole water, the Mowbray River and the CPUT tap water were used without any pretreatment. The samples were first filtered and mixed with 0.1M KOH electrolyte solution (pH=12). The water samples were spiked with NO_3^-. CV method was employed to electrochemically detect nitrate, at optimum conditions.

3.2.4 Physical characterization

The crystal structure of Cu_xO and Sn-Cu_xO thin films were examined by X-ray diffraction (XRD, PANalytical X'Pert PRO PW3040/60) technique where XRD patterns were obtained in the 2 theta range of 20–40° using Cu-Kα radiation of wavelength λ = 0.154 nm with the step size of 0.02 °/s. SEM micrographs of the thin films were obtained by using Tescan MIRA3 RISE SEM, a high-resolution Field Emission SEM that is associated with low kV imaging Nova Nano SEM. XPS measurements were carried out on Cu_xO and Sn-Cu_xO with spatial resolution of < 3 µm using KRATOS AXIS X-ray photoelectron spectrometer at UNISA (Florida Science Campus), South Africa.

3.2.5 Electrochemical characterization

All electrochemical measurements were carried out using Autolab PGSTAT204 potentiostat with pre-installed NOVA 2.1 software. The conventional three-electrode setup was adopted with Ag/AgCl/KCl (3 M) as the reference electrode, Platinum wire as counter electrode, and Cu_xO/Sn-Cu_xO as working electrodes. Cyclic voltammetry (CV) and chronoamperometry (CA) experiments were performed at room temperature in 40 mL of 0.1 M KOH. EIS study was conducted using 5 mM K_4 [Fe (CN) $_6$]/K_3 [Fe (CN) $_6$] as the redox probe in 0.1 M KCl over the frequency range of 1 - 100 kHz and ac voltage amplitude of 100 mV. The Randles equivalent circuits were obtained using EIS Spectrum Analyser.

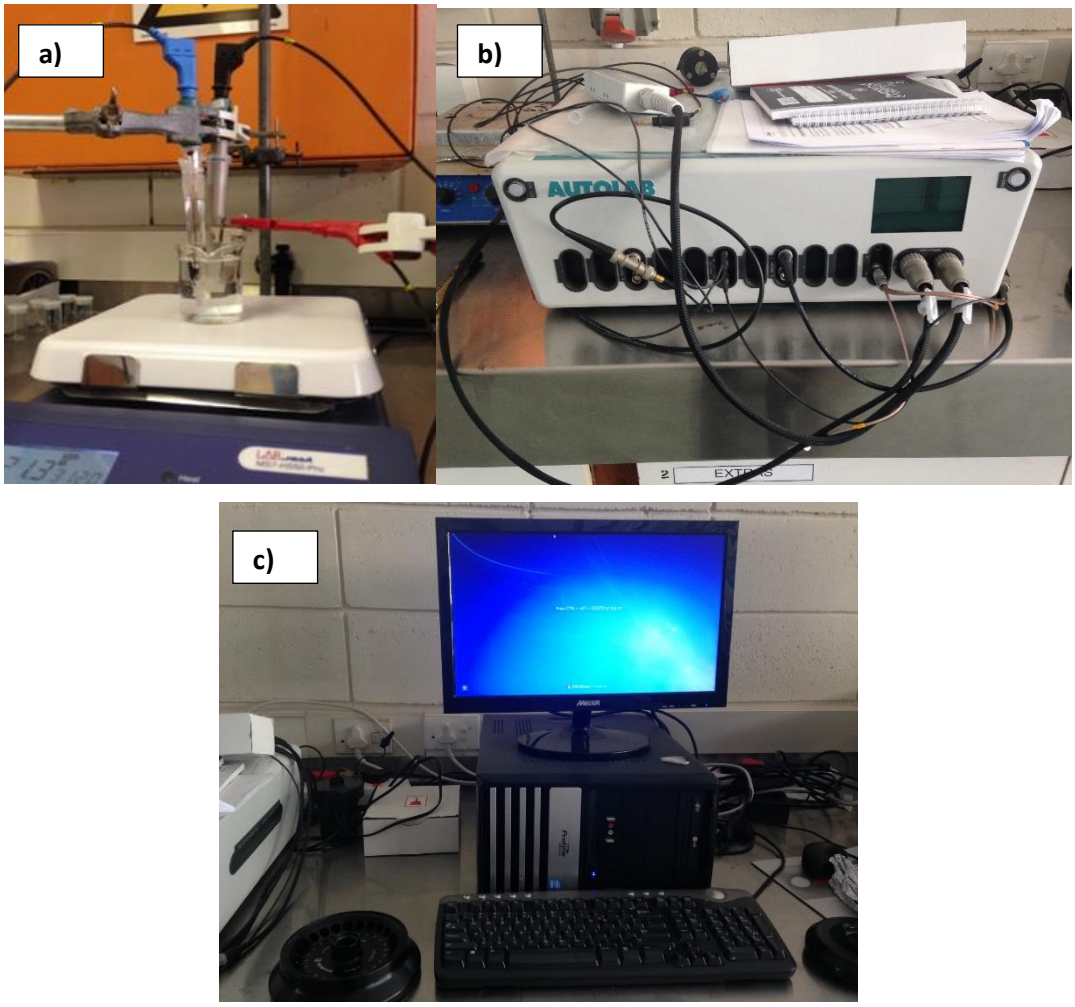

Figure 3.2: Electrochemical measurements with a) Electrochemical cell b) Auto lab PGSTAT204 and c) Data collection Nova 2.1

3.3 Conclusion

This chapter outlines the research methods and techniques employed in the study, offering insights into the materials, procedures, and instruments used for data collection and analysis. The electrode fabrication process involves the synthesis of copper oleate, deposition of undoped and Sn-doped Cu_xO thin films, and their subsequent calcination.

Real samples preparation for environmental testing included Bore hole water, Mowbray River water, and CPUT tap water, filtered and mixed with 0.1M KOH electrolyte solution. The water samples were spiked with NO_3^-, and cyclic voltammetry (CV) was employed for electrochemical nitrate detection.

Physical characterization involved examining the crystal structure of Cu_xO and Sn-Cu_xO thin films using X-ray diffraction (XRD) and obtaining SEM micrographs. XPS measurements were carried out for spatial resolution. Electrochemical characterization was conducted using Autolab PGSTAT204 potentiostat with cyclic voltammetry, chronoamperometry, and electrochemical impedance spectroscopy (EIS) experiments.

The research utilized a comprehensive approach, integrating material synthesis, characterization techniques, and electrochemical analysis to investigate the properties of Cu_xO and Sn-Cu_xO thin films and their application in nitrate detection in water samples.

Chapter 4 : Results and Discussion

4.1 Introduction

This chapter discusses in detail the results and analysis obtained throughout the experiment. The structural analysis and physical characterization of the catalysts used were presented to establish a comparative study between the pristine Cu_xO and Sn-Cu_xO nanocomposite thin films. The electrochemical characterization of the catalysts in order to study the current response between the elements is also presented in this section. The methods used are XRD, SEM, XPS, CV, CA, and EIS. The findings are also discussed based on the previous research findings and literature.

Real sample study is also performed and examined where different type of analyte were used.

4.2 Physical characterization

4.2.1 X-ray diffraction (XRD) analysis

XRD is a non-destructive technique used to identify the crystalline phase present in a material and provides chemical composition information. XRD was used to confirm the joining of the cubic Cu_2O and monoclinic CuO phases as well as Sn doping.

The XRD pattern of Cu_xO in Figure 4.1 (red curve) showed diffraction peaks at angles such as 2θ=31.75, 33.99, 35.63, 38.08, and 38.76º that corresponded, respectively, to the standard crystal directions of CuO(110) (SoYoon et al., 2014), CuO(-111) (Felix et al., 2018), Cu_2O(111) (Balık et al., 2019), CuO(111) (Bin Mobarak et al., 2022), and Cu_2O(200) (Balık et al., 2019). The crystal planes obtained are the most intense XRD signals with almost equal magnitude as the preferred growth orientations. No other impurity phases were detected. The occurrence of a dual phase in this study, unlike previously, resulted from the adjustment of the spin-coating time. A decreased spin-coating time led to a thicker film, which meant a higher mass loading and therefore an increased number of Cu^+ ions that were favourable to the partial oxidation of Cu_2O to CuO.

The influence of Sn doping on the crystal structure of Cu_xO thin film can be seen in Figure 4.1 (black curve) with **a)** the enhanced growth of CuO along the (110) axis, **b)** the peak splitting at 2θ = 38.76º showing phase transition of Cu_2O from cubic to the tetragonal shape (Fan and Kim, 2001), and **c)** the disappearance of the CuO(-111) and (111) XRD peaks, denoting a loss of crystallinity and the introduction of amorphous domains due to lattice distortion (Pal et al., 2012). These significant crystallographic changes of the CuO peaks after Sn doping seemed

to suggest that Sn^{4+} had entered the CuO lattice through substitutional doping. This is most likely as the ionic size of Sn^{4+} (0.69 A) is close to that of Cu^{2+} (0.72 A). No Sn^{0}, SnO, SnO_2, or residual $SnCl_2$ phase was found, meaning that Sn was successfully incorporated into the lattice structures of Cu_xO.

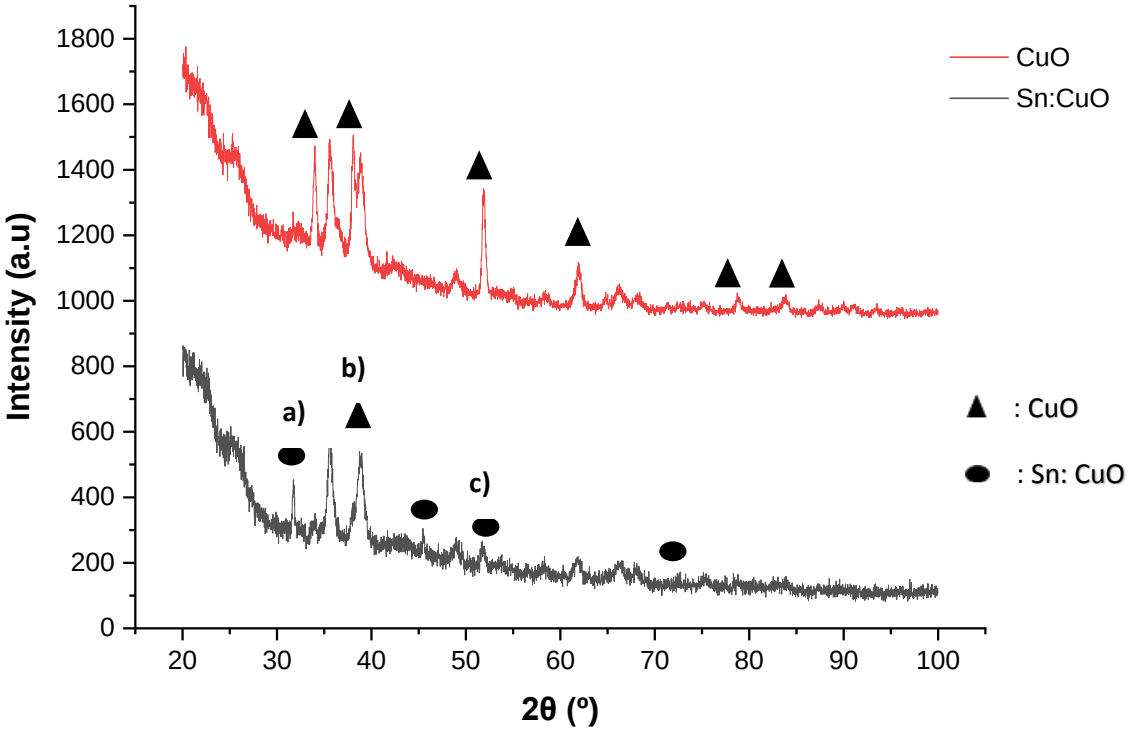

Figure 4.1: XRD Pattern of Cu_xO / Sn: Cu_xO

4.2.2 Scanning electron microscopy (SEM) analysis

Undoped and Sn-doped Cu_xO thin films were characterized by SEM to gain information about their surface morphology. Their corresponding micrographs are shown in Figure 4.2a-b and Figure 4.3c-d, respectively with (a, c) depicting a low-magnification image and (b, d) a high-magnification image of the undoped and Sn-doped Cu_xO structure.

The images clearly show that the films have good contact between the substrate and the coating. Clear changes in the surface morphology of the Cu_xO/FTO electrode were observed. The surface morphology of Cu_xO thin film showed the predominance of regularly shaped, single, and clustered ice cube-like crystals. Upon doping of Sn, one could pick up the emergence of irregularly shaped and quasi-cubic structures, which demonstrated structural changes and a decrease in crystallinity as substantiated by the XRD results of Sn-Cu_xO thin film.

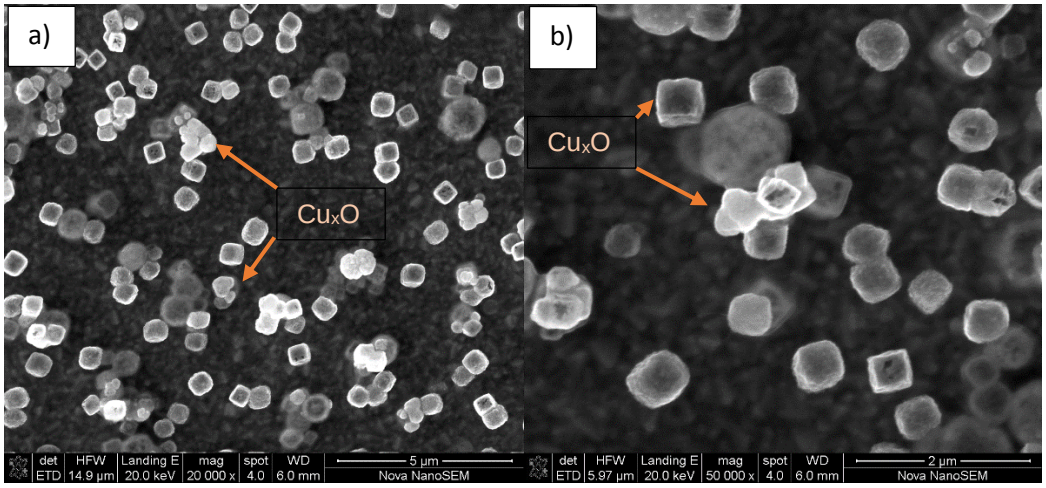

Figure 4.2: SEM images of undoped Cu_xO with (a) depicting a low-magnification image and (b) a high-magnification image of the undoped Cu_xO structure.

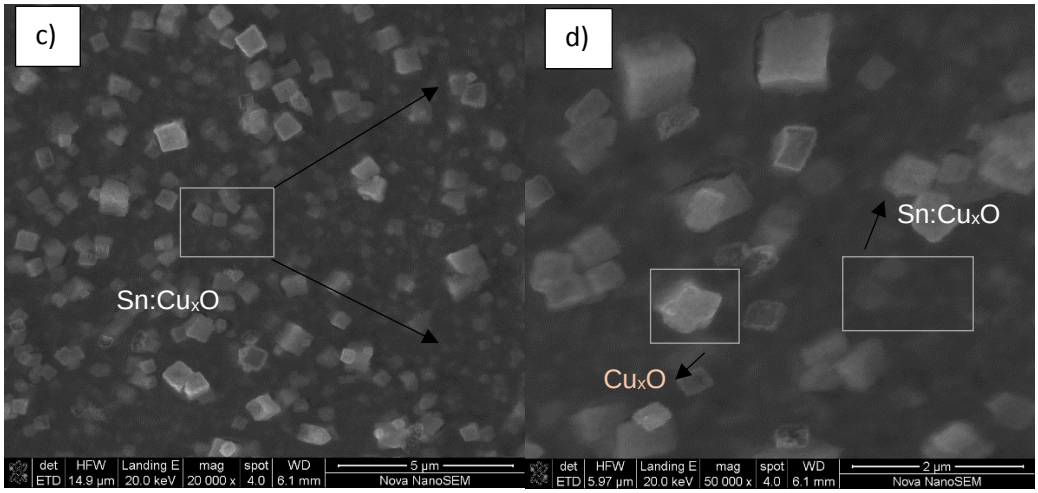

Figure 4.3: SEM images of Sn-doped Cu_xO structure with (c) depicting a low-magnification image and (d) a high-magnification image of Sn-doped Cu_xO.

4.2.3 X-ray photoelectron spectroscopy (XPS) analysis

XPS experiments were performed on Cu_xO and Sn-Cu_xO thin films to examine their surface chemistry. All spectra were analysed using OriginPro software and referenced at 284.8 eV for adventitious carbon. More attention was devoted in this research to the analysis of the Cu $2p_{3/2}$, Sn $3d_{5/2\text{-}3/2}$, and O 1*s* spectra. Other material analysis are for supplementary information.

Deconvolution of the Cu $2p_{3/2}$ XPS spectrum of Cu_xO thin film showed two spectral peaks (see Figure 4.4) centred at 932.8 and 934.6 eV for Cu^+ (Cu_2O) (Wang et al., 2011) and Cu^{2+} (CuO) (Ahmed et al., 2016) respectively. This thus confirmed the presence of both Cu_2O and CuO phases (Cu^{2+}/Cu^+ = 0.7/1.4) on the surface of the film and corroborated with XRD results. The satellite peak near 942.5 eV was attributed to the paramagnetic Cu^{2+} ions (Zeng et al., 2003).

Sn doping caused noteworthy spectral changes of the Cu $2p_{3/2}$ XPS band of Cu_xO thin film. Specifically, the Cu^{2+}/Cu^+ spectral ratio dropped to 0.4/1.4, indicating a decrease of the number of Cu^{2+} ions due to substitutional Sn^{4+} ions as per XRD. In addition, the replacement of a single Cu^{2+} cation by one Sn^{4+} ion necessitated the generation of a Cu^{2+}-vacancy due to the charge difference between the host and guest ions to maintain the condition of electro neutrality (See Equation 7). The release of Cu^{2+} ions after Sn^{4+} doping was proposed to be responsible for the enhanced growth of CuO along the (110) axis (See Equation 8) in agreement with the XRD data of Sn-Cu_xO. For site balance, substitutional Sn^{4+} ion and resulting Cu^{2+}-vacancy liberate two free electrons as per Equation 9 (these free electrons can tune the electronic properties of Sn-Cu_xO) and two free holes (See Equation 10), respectively. The formation of Sn^{4+}-induced Cu^{2+} vacancies accounted also for the reduction of the number of Cu^{2+} cations and blue shifts (by 0.3-0.4 eV) of the XPS peaks of Sn-Cu_xO thin film as a result of a decrease in the electronic density (See Figure 4.5).

Also, one could notice a reduced peak intensity of the satellite feature at 942.9 eV, confirming the depletion of Cu^{2+} ions. No change in the amount of Cu^+ cations was observed after Sn doping. To ascertain the oxidation states of Sn, deconvolution of the Sn $3d_{5/2\text{-}3/2}$ bands was performed, which accused of the presence of both Sn^{4+} and Sn^{2+} ions in the spectral ratio of 0.4/1.0. Indeed, Sn^{4+} substituted Cu^{2+} as suspected. On a 100 % basis of the total number of elements present on the surface of Cu_xO and Sn-Cu_xO thin films, the depleted amount of Cu^{2+} ions (by 0.3 %) in Sn-Cu_xO was found to be disproportional to that of Sn^{4+} (0.4 %), and this

suggested that the excess dopant atoms i.e., Sn^{4+} and Sn^{2+}, possibly occupied the interstices of the cubic Cu_2O and/or monoclinic CuO phase(s). This could then explain the phase transition (from cubic to the tetragonal geometry) mentioned earlier for Cu_2O based on XRD.

The O 1*s* XPS results of Cu_xO in Figure 4.4 & 4.5 showed peaks at 529.7, 531.2, and 532.9 eV which were assigned to the lattice oxygen (O^{2-} = $\mathbf{O_{Latt}}$) of CuO, lattice oxygen (O^{2-}) of Cu_2O/carbonaceous oxygen, and chemisorbed oxygen ($\mathbf{O_{Ads}}$), respectively. Correction of the O 1*s* XPS photo peak at 531.2 eV could be applied to separate between the contribution of the Cu_2O lattice oxygen and that of carbon-related oxygen (Ciftyürek et al., 2019).

The ratio of $\mathbf{O_{Ads}}/\mathbf{O_{Latt}}$ (2.4/2.3) was used to probe the surface oxygen vacancies of the CuO phase. Sn doping of Cu_xO resulted in the concomitant decrease and increase of the O 1*s* XPS peaks at 530.0 and 533.2 eV, respectively, as in Figure 4.5. This strange and unexpected change was rationalized to be the resultant of an augmented amount of oxygen vacancies ($\mathbf{O_{Ads}}/\mathbf{O_{Latt}}$ = 4.3/1.1) in CuO after substitution of Sn^{4+} by Cu^{2+}. In general, the substitutional doping with low-valent cations instead yields oxygen vacancies owing to the electro neutrality principle. The tabulated XPS results of O 1*s,* Cu 2*p*, and Sn 3*d* are presented in Table 4.1 below.

Table 4.1: Tabulated summary of O 1s, Cu 2p, and Sn 3d XPS results

Electrode	O_{Ads}/O_{Latt}	Cu^{2+}/Cu^{+}	Sn^{4+}	Sn^{2+}
Cu_xO	2.4/2.3	0.7/1.4	-	-
Sn-Cu_xO	4.3/1.1	0.4/1.4	0.4	1.0

Furthermore, the increase of oxygen vacancies is often related to an increase of low-valent cations as previously observed (Ndala et al., 2021). However, this is not the case here. Although more oxygen vacancies were formed, the number of Cu^{+} ions remained unchanged. Further investigations were conducted, and it was concluded that the oxygen vacancies originated from the reaction between the holes produced by Cu^{2+} vacancies and the neighbouring lattice oxygen species (See Equation 11): the generation of oxygen vacancies is always succeeded by the release of two electrons, which recombined in this case with two holes of Cu^{2+}-vacancy and vanished, thereby preventing the increase of Cu^{+} ions through electron trapping in the 3*d* orbitals of Cu^{2+}. The XPS peaks of Sn-Cu_xO thin film at 530.0 and 533.2 eV appear positively shifted (by 0.3 eV) compared to those of Cu_xO thin film because of reduced electron density emanating from the decrease of the amount of CuO lattice oxygen.

$$SnCl_2.2H_2O \xrightarrow{O_2} \left(\frac{Sn^{4+}}{Sn^{2+}}\right) = 0.4 \quad (6)$$

$$(Sn^{4+} + Cu_{Cu})_{CuO} \xrightarrow{\Delta} \left(Sn_{Cu}^{2+} + V_{Cu}''\right)_{CuO} + 2Cu^{2+} \quad (7)$$

$$Cu^{2+} \xrightarrow{\text{Enhanced growth}} CuO(110) \quad (8)$$

$$Sn_{Cu} \rightarrow Sn_{Cu}^{2+} + 2e' \quad (9)$$

$$V_{Cu} \rightarrow V_{Cu}'' + 2h^{\bullet} \quad (10)$$

$$O_o + 2h^{\bullet} \rightarrow \frac{1}{2}O_2 + V_o^{\bullet\bullet} \quad (11)$$

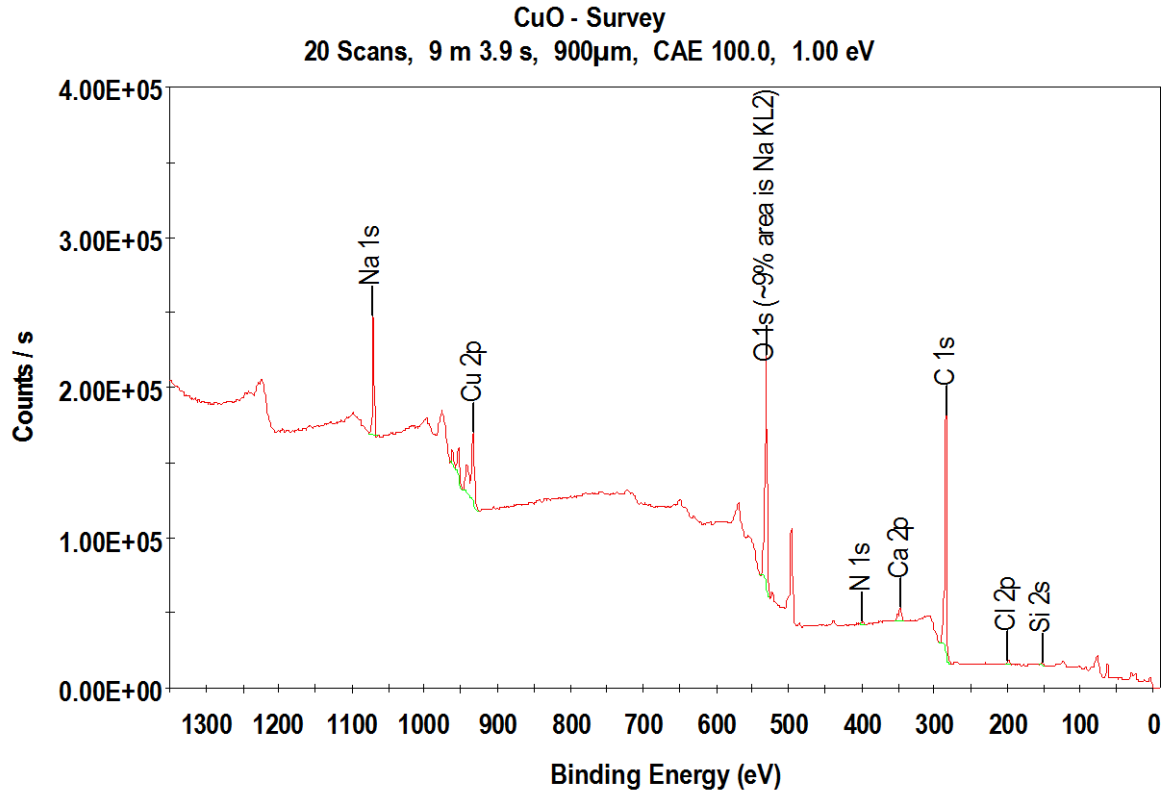

Figure 4.4: XPS survey of Cu_xO

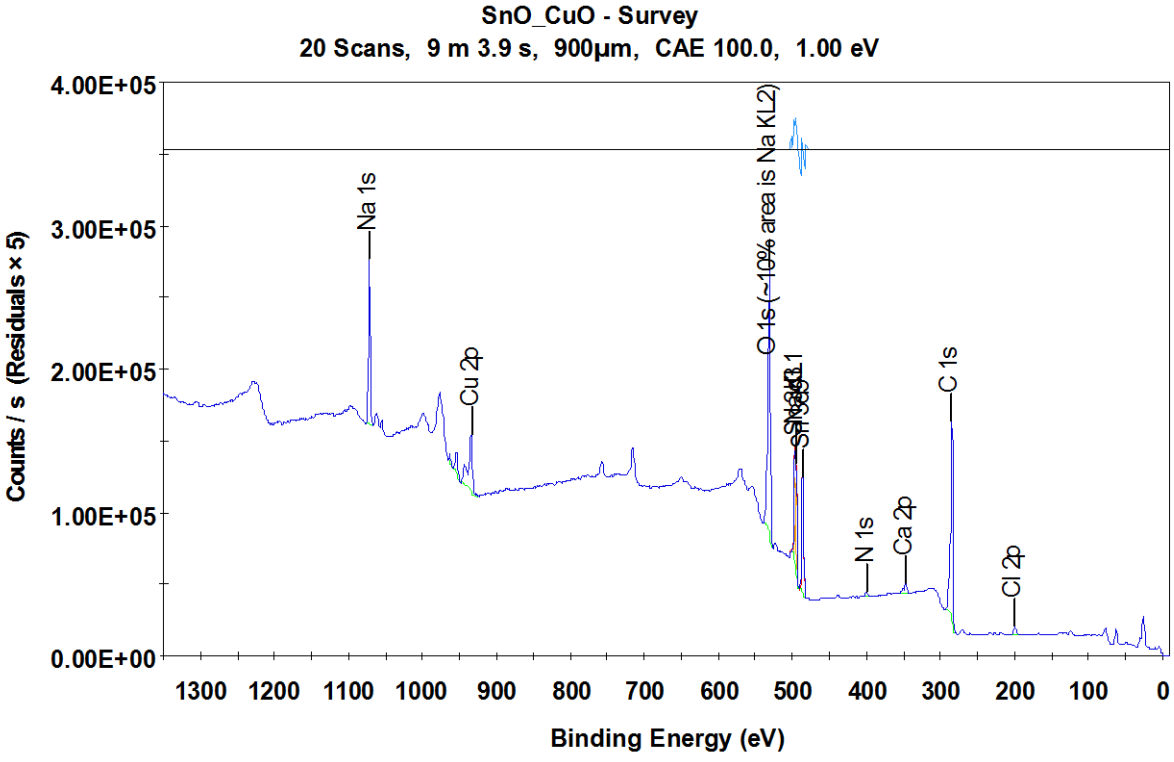

Figure 4.5: XPS survey of Sn/Cu_xO

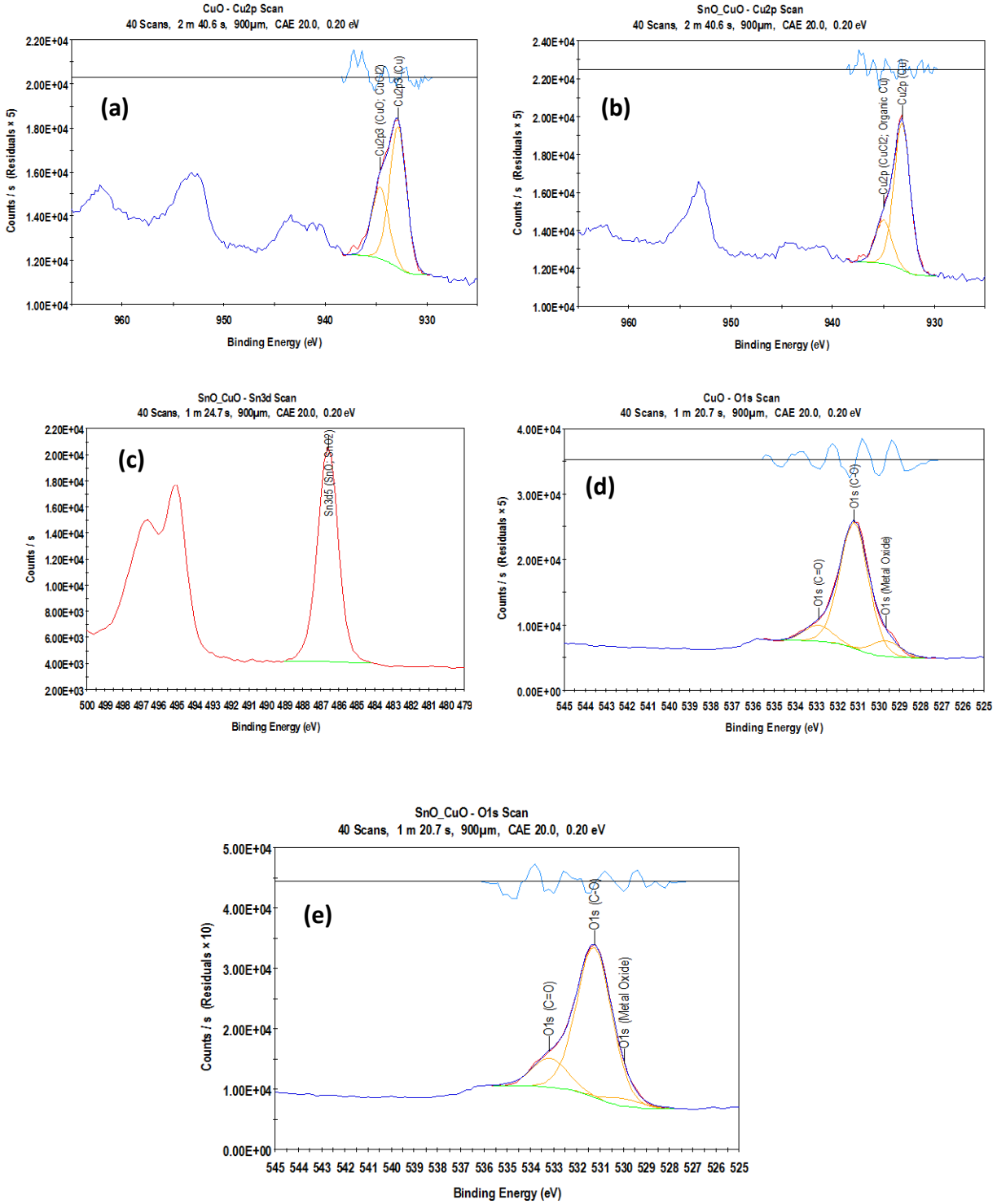

Figure 4.6: Full scan XPS spectrum (a) Cu 2p of pristine Cu_xO,(b) Cu 2p of Sn-Cu_xO, (c) Sn 3d of Sn-Cu_xO (d) O 1s of pristine Cu_xO (e) O 1s of and Sn-Cu_xO.

Table 4.2: Sn-doped Cu_xO elemental composition

Name	***Peak BE***	***Atomic %***
C 1s	284.9	58.4
O 1s (~10% area is Na KL2)	531.3	30.2
Na 1s	1071.8	6.1
Cu 2p	934.1	2.0
Sn 3d5	486.4	1.3
Cl 2p	199.7	0.9
N 1s	400.0	0.6
Ca 2p	347.0	0.6

Table 4.3: Cu_xO elemental composition

Name	***Peak BE***	***Atomic %***
C 1s	284.4	65.5
O 1s (~9% area is Na KL2)	531.0	24.7
Na 1s	1070.7	4.9
Cu 2p	933.6	2.8
Ca 2p	347.1	0.8
Si 2s	152.5	0.5
Cl 2p	198.8	0.4
N 1s	398.8	0.3

4.3 Electro catalytic performance of the as prepared electrodes

4.3.1 Cyclic voltammetry (CV)

The electrochemical activity of Sn-Cu_xO/FTO, Cu_xO/FTO and bare FTO was further evaluated and compared for the detection of 1 mM NO_3^- in 0.1 M KOH electrolyte at 30 mV/s. Figure 4.6 shows the cyclic voltammograms of Sn-Cu_xO/FTO obtained in the range of -1.2 to 0.1 V (vs. Ag/AgCl) . In a blank 0.1 M of KOH solution, without any nitrate addition, no obvious peak appeared between -1.2 and -0.9 V (vs. Ag/AgCl), while in the solution containing 1mM of NO_3^- an intense reduction peak appeared in the cathodic scan with no reversible anodic peak. Thus, the peak at -1V indicates the reduction of nitrate.

In figure 4.7 the outcome of the CV experiment, revealed that Sn-Cu_xO showed the best electro catalytic response with the highest cathodic peak current of NO_3^- occurring by -1 V compared to that of pristine Cu_xO. No redox peaks were observed at bare FTO. The improved performance of Sn-Cu_xO/FTO compared to that of Cu_xO/FTO was assigned to the incorporation of Sn into Cu_xO lattice. Specifically, the surface free electrons supplied from substitution of Cu^{2+} by Sn^{4+} could participate in conduction during nitrate electro reduction and result in enhanced current signal of Sn-Cu_xO thin film.

In both figures (4.6 & 4.7), it shown the cyclic voltammograms of Sn-Cu_xO thin film swept in the range of -1.2 to 0.1 V at the scan rate of 30 mV/s in blank and 1 mM nitrate-containing KOH. Without nitrate addition (blank), two cathodic peaks (III, IV) were found at -0.34 and -0.75 V, and the corresponding anodic peak (I, II) currents were noticed at -0.125 and -0.34 V, these indicate the reduction and oxidation attributed to the pairs of Cu(II)/Cu(I) (See Equation 12) and Cu(I)/Cu(0) (See Equation 13), respectively.. These redox peaks confirmed the coalescence of the Cu_2O and CuO phases. In 1 mM nitrate, the magnitude of the cathodic and anodic peak currents of the Cu(II)/Cu(I) and Cu(I)/Cu(0) couples decreased significantly due to analyte adsorption, and the reduction peak current of nitrate appeared at -1 V (vs. Ag/AgCl). The fact that nitrate electro reduction took place shortly after the reduction peak current of the Cu (I)/Cu (0) couple suggested that the metallic Cu^0 provided activation for the reduction process (Amertharaj et al., 2014).

$$2CuO + H_2O + 2e^- \rightarrow Cu_2O + 2OH^- \qquad (12)$$

$$Cu_2O + H_2O + 2e^- \rightarrow 2Cu^* + 2OH^- \qquad (13)$$

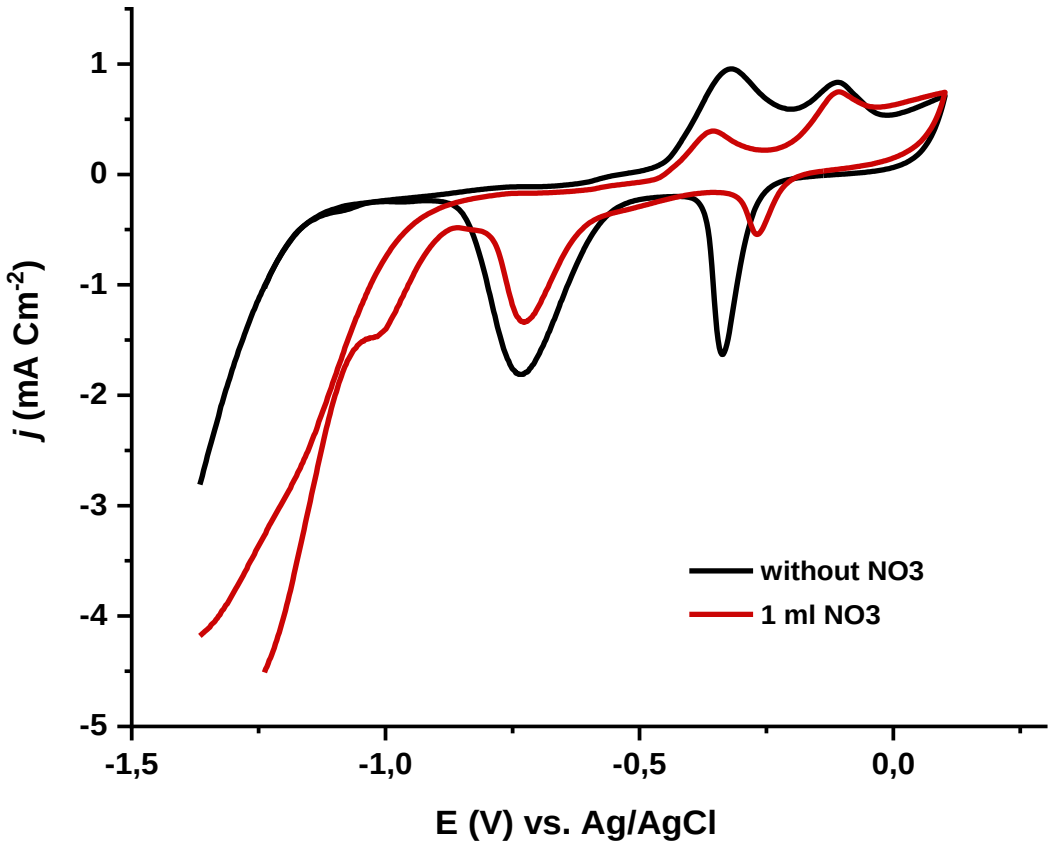

Figure 4.7: Cyclic voltammograms of Sn-Cu_xO/FTO in a blank solution and in the presence of 1ml of NO3-

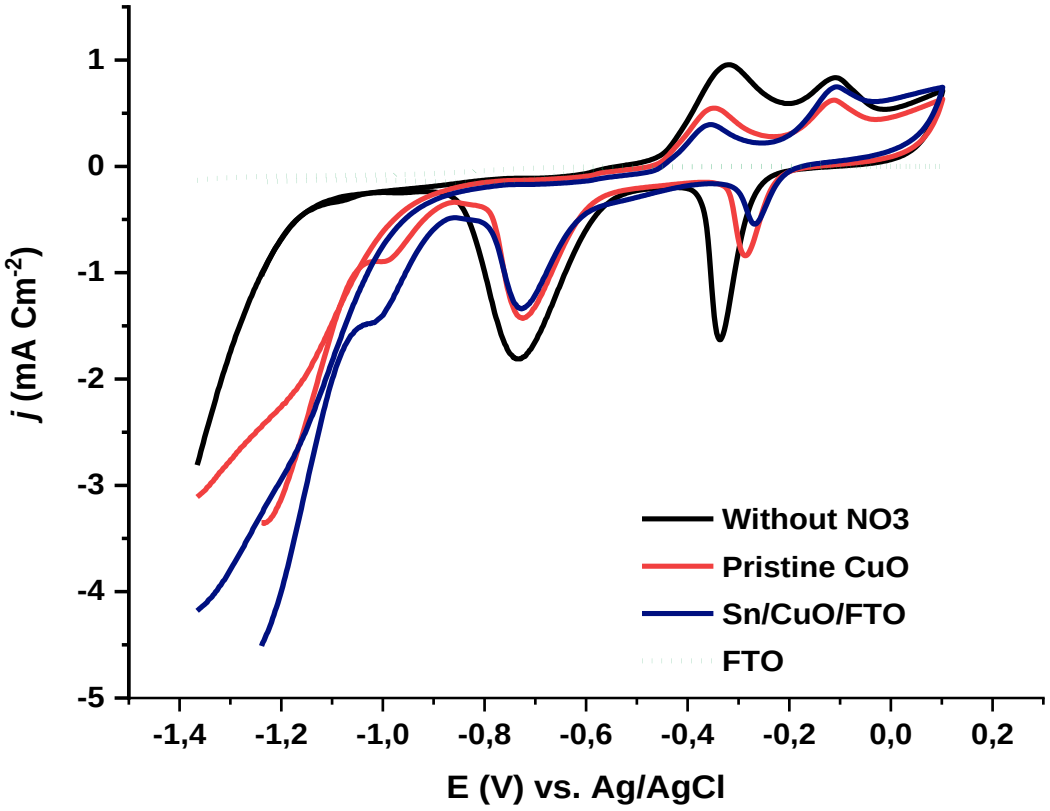

Figure 4.8: Cyclic voltammograms of Sn-Cu_xO/FTO, Cu_xO/FTO and bare FTO in a blank solution and in the presence of 1ml of NO_3^-

Figure 4.8 exhibits the CV curves of Sn-Cu_xO thin film in 0.1 M KOH electrolyte solution with successive additions of nitrate. The inset of the figure shows a linear increase of cathodic peak current with nitrate concentration varying from 1 - 4 mM (correlation coefficient R^2 = 0.9964) (Figure 4.9) is observed and this confirmed the nitrate-sensing capability of the Sn-Cu_xO thin film. In addition, the cathodic peak potential shifted negatively with increasing nitrate concentration due to nitrate adsorption on the electrode surface (Jasna et al., 2020).

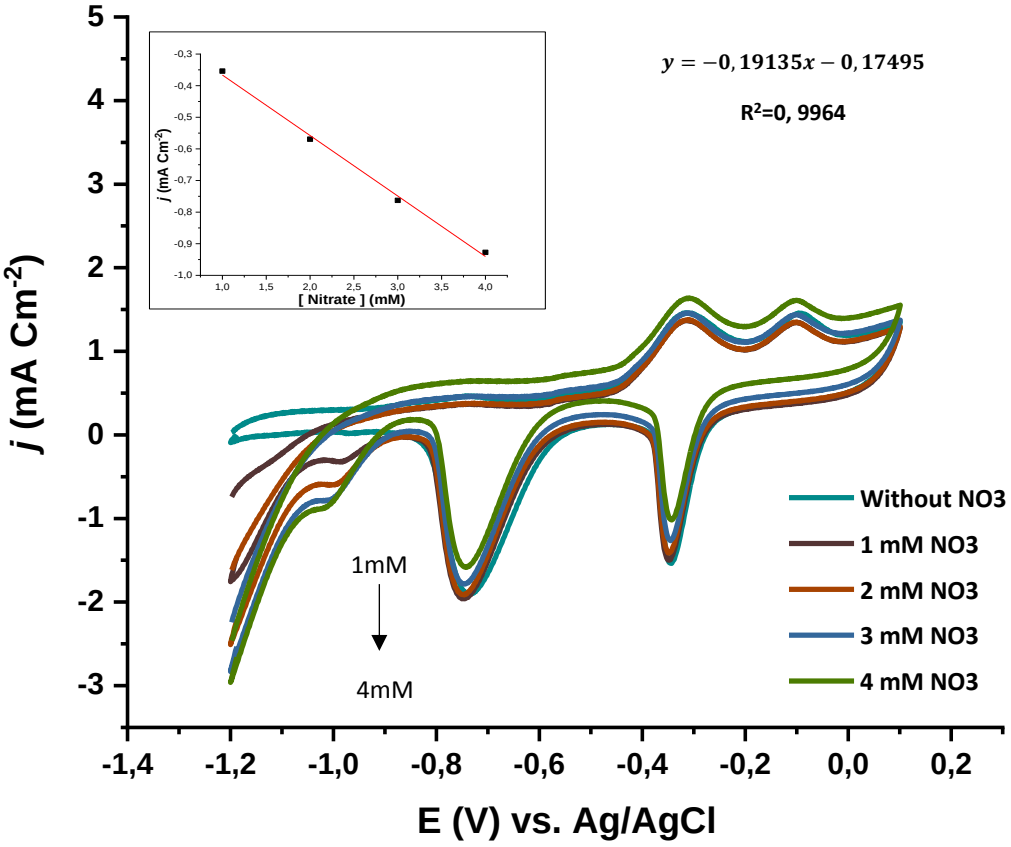

Figure 4.9: CV curves of Sn-Cu_xO thin film in 0.1 M KOH electrolyte solution with successive additions of nitrate

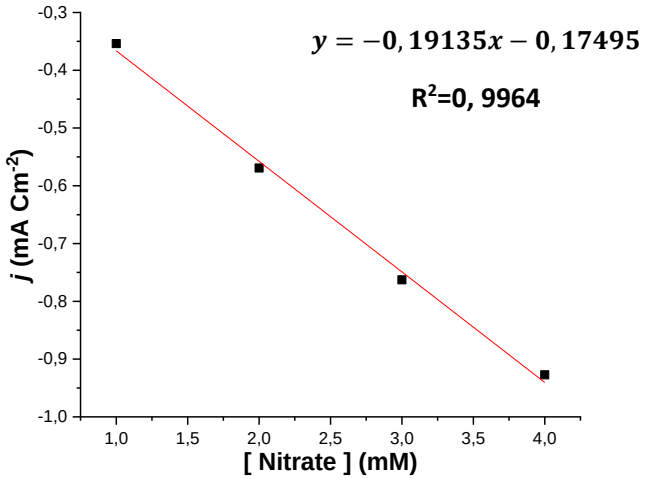

Figure 4.10: Peak current vs nitrate concentration calibration graph

4.3.2 Effect of scan rate

Figure 4.10 illustrates the effect of scan rate on the cyclic voltammogram (CV) of Sn-Cu_xO thin film in 1 mM nitrate electrolyte solution at the scan rate range of 25-200 mV/s. Figure 4.11 demonstrates the linear relationship between cathodic peak current of NO_3^- and scan rate (correlation coefficient $R^2 = 0.9986$). This straight trend is inherent to an adsorption-controlled process. The cathodic peak potential shifted in the negative direction with increasing scan rate due to the chemical irreversibility of the electro reduction process (Fox and Breslin, 2020), as seen in Figure 4.10. The product $(\alpha_c n_c)$ was found from Equation 14 (Aristov and Habekost, 2015) (to calculate the standard electron-transfer rate constant k^0) with E_p and $E_{p/2}$ as the cathodic peak and half-peak potentials (V), respectively. Hence, $(\alpha_c n_c)$ in case of Cu_xO and Sn-Cu_xO was found to be 0.96 and 0.76, respectively.

$$E_p - E_{\frac{p}{2}} = \frac{0.0477}{(\alpha_c n_c)} \qquad (14)$$

The k^0 values for Cu_xO and Sn-Cu_xO were calculated from Equation 15 (Aristov and Habekost, 2015) and were found to be 337 and 391 s^{-1}, respectively.

$$E_P = E^{0\prime} + \frac{RT}{(\alpha_c n_c)F}\ln\left(\frac{RTk^0}{\alpha_c n_c F}\right) - \frac{RT}{(\alpha_c n_c)F}\ln v \qquad (15)$$

Where $E^{0\prime}$ is the formal electrode potential (V), obtained using the cyclic voltammograms of Cu_xO and Sn-Cu_xO in Figure 4.6, R is the gas constant (8.314 J/mol.K), F is the Faraday's law constant (96485 C), T is the temperature in K, and v is the scan rate in V/s. α_c is the transfer coefficient, and n_c is the number of electrons transferred in the rate-determining step.

The number of transferred electrons was further calculated using the cathodic peak current ratio of nitrate from the cyclic voltammograms of Sn-Cu_xO and Cu_xO as described in Equation 18, derived from the mathematical manipulation of Equations 16 & 17 below for adsorption-controlled irreversible process (Aristov and Habekost, 2015):

$$I_{PC} = \frac{(\alpha_c n_c){n_c}^2 F^2 \Gamma A v}{2.718RT} \qquad (16)$$

$$\Gamma = \frac{Q}{n_c FA} \qquad (17)$$

$$\frac{I_{PC/1}}{I_{PC/2}} = \frac{(\alpha_c n_c)_{/1} n_{c/1} Q_{c/1}}{(\alpha_c n_c)_{/2} n_{c/2} Q_{c/2}} \qquad (18)$$

Where $I_{PC/1}$ and $I_{PC/2}$ are the cathodic peak currents of Sn-Cu_xO and Cu_xO, respectively, obtained from their respective cyclic voltammograms. We observed a two-fold enhancement in reduction peak current of nitrate at the Sn-Cu_xO electrode. $Q_{c/1}$ And $Q_{c/2}$ are the integrated peak areas of the Sn-Cu_xO and Cu_xO electrodes, respectively, from their CV spectra. Γ Is the surface concentration of the electroactive analyte. The number of electrons transferred for Cu_xO and Sn-Cu_xO was found to be 1 and 2, respectively.

The mechanism of nitrate reduction at Cu_xO and Sn-Cu_xO includes electrons transfer process leading to the formation of a range of intermediates and final products depending on experimental factors, such as the material used to modify the electrode, the supporting electrolyte used, the pH of the medium, and the applied electric potential. According to the literature, a step-wise reaction mechanism is widely accepted, in which nitrate is first reduced to intermediate nitrite as the rate-determining step, followed by further reduction of nitrite to possible end products at over potential. According to (Siddiqui et al., 2021), the nitrate reduction involves adsorption of NO_3^- ions onto the active sites of the electrochemically produced Cu^0 species (Equations 20 & 24), which in turn mediated the electro reduction of NO_3^- by supplying electrons to produce cuprous ions (Equations 21 & 25). Finally, the Cu^+ ions instantly got reduced to restore the metallic Cu by a flow of current from the external circuit (e^-_{ext}) (Equations 22 & 26). NO_3^- is first adsorbed on the surface of the Sn/Cu_xO/FTO, and then the reduction of NO_3^- to NO_2^- on the surface of the electrode exhibited a two-electron transfer process. The main difference in nitrate reduction pathway between the sensors was the one- and two-electron transfer for Cu_xO and Sn-Cu_xO, respectively, leading to two different products, i.e. NO_2 (for Cu_xO) and NO_2^- (for Sn-Cu_xO). The increased number of electrons

transferred in the case of Sn-Cu_xO was assigned to the excess/surface free electrons derived from substitutional Sn^{4+} doping. To outline the electronic contribution of Sn^{4+} doping, one electron (e^-_{surf}) was added to the left-hand side of Equation 25 for a total of two transferred electrons (i.e., one from the metallic Cu and the other from the dopant).

The reaction describing the electro catalytic reduction of nitrate in the alkaline medium in the figures and explanations above can be illustrated by:

<u>Cu_xO</u>

$$\frac{1}{2}Cu_2O + \frac{1}{2}H_2O + e^- \rightarrow Cu^* + OH^- \quad (19)$$

$$Cu^* + NO_{3\,(aq)}^- \leftrightarrow Cu^*(NO_3^-)_{ads} \quad (20)$$

$$Cu^*(NO_3^-)_{ads} + H_2O \rightarrow Cu^+(NO_2)_{ads} + 2OH^- \quad (21)$$

$$Cu^+(NO_2)_{ads} + e^-_{ext} \rightarrow Cu^*(NO_2)_{ads} \quad (22)$$

<u>Sn-Cu_xO</u>

$$\frac{1}{2}Cu_2O + \frac{1}{2}H_2O + e^- \rightarrow Cu^* + OH^- \quad (23)$$

$$Cu^* + NO_{3\,(aq)}^- \leftrightarrow Cu^*(NO_3^-)_{ads} \quad (24)$$

$$Cu^*(NO_3^-)_{ads} + H_2O + e^-_{surf} \rightarrow Cu^+(NO_2^-)_{ads} + 2OH^- \quad (25)$$

$$Cu^+(NO_2^-)_{ads} + e^-_{ext} \rightarrow Cu^*(NO_2^-)_{ads} \quad (26)$$

Overall reaction: $NO_3^- + H_2O + 2e^- \rightarrow NO_2^- + 2OH^-$ (Mumtarin et al., 2020)

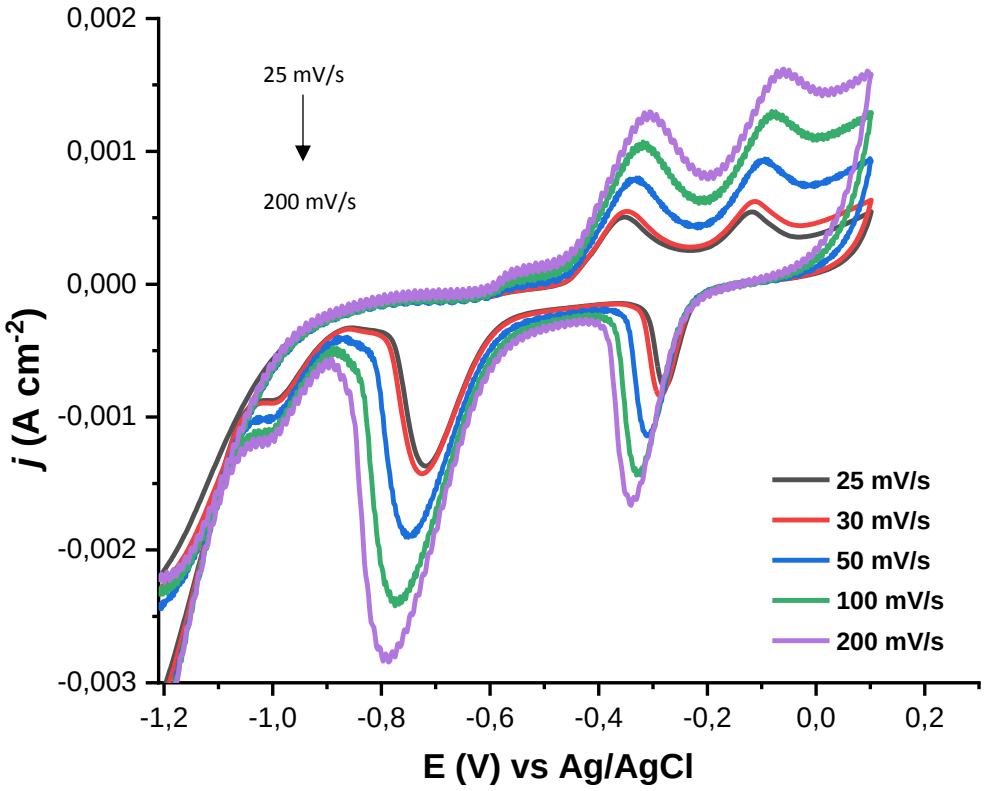

Figure 4.11: Effect of scan rate

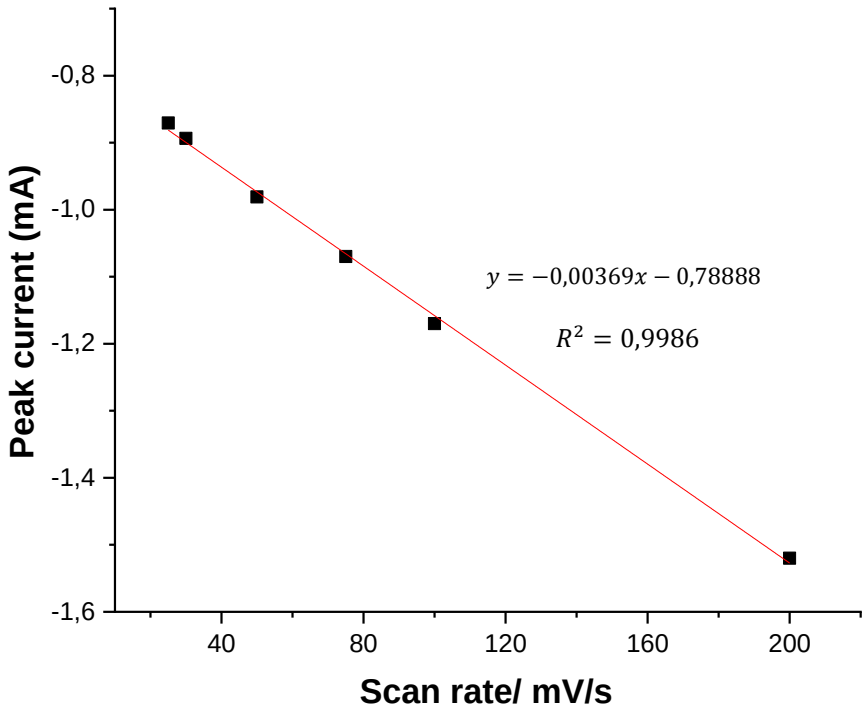

Figure 4.12: Peak current vs scan rate calibration graph

4.3.3 Chronoamperometric study of the as prepared electrode

4.3.3.1 Chrono amperometry (CA)

The performance parameters of Sn-Cu_xO thin film were further evaluated using amperometric (peak current versus time) responses. Figure 4.12 shows the I–t responses of the Sn-Cu_xO thin film upon consecutive additions of nitrate in 0.1 M KOH electrolyte solution under mild stirred conditions near -1 V (vs. Ag/AgCl). The corresponding inset displays the plots of current values as a function of nitrate concentration with a good linear range of 0.01 - 15 mM. The linear regression equation is I_p (mA/cm^2) = −0.10027 C (mM) - 0.0911, where I_p is the current density (mA/cm^2) and C the nitrate concentration (mM), with a correlation coefficient R^2 of 0.9956. The sensitivity of the device was found to be 100.27 µA.mM^{-1}.cm^{-2}. Additionally, the limit of detection (LOD) was estimated to be 0.04 µM (S/N = 3) and was calculated from the equation:

$$LOD = \frac{3 \times SD}{m} \quad (28)$$

Where, 'SD' is the standard deviation of the current response and 'm' the slope of the calibration curve.

The LOD calculated (0.04 µM) was considerably lower than the maximum allowable NO_3^- concentration in drinking water according to the WHO regulation and confirmed the practical application of Sn-Cu_xO. On the basis of the obtained results, it is clearly established that the performance of the nitrate sensor developed in this work has better sensitivity and exhibited the lowest detection limit than that reported in Table 4.2 and to the enzymatic and non-enzymatic electrochemical nitrate sensors based on graphene derivatives, carbon nanotubes/fibers, metal/bimetal/metal oxide, and conducting polymers reported in a recent publication review (Amali et al., 2021).

.

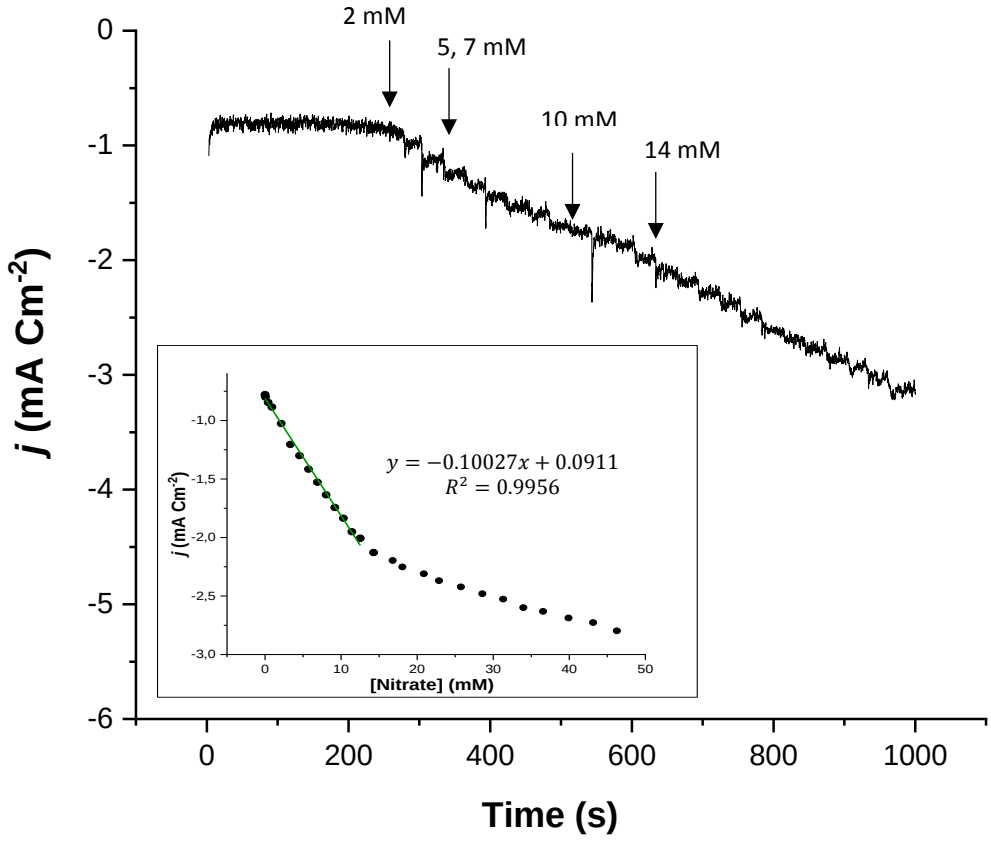

Figure 4.13: Chrono Amperometry of Sn-Cu_xO/FTO upon consecutive additions of nitrate in 0.1 M KOH electrolyte

4.3.3.2 Interference study

The selectivity of the Sn-Cu_xO sensor was studied using chronoamperometry in 0.1 M KOH electrolyte with consecutive addition of a steady amount of nitrate at an applied over potential of -1 V in the presence of 5-times higher concentrations of possibly interfering anions present in water such as nitrite, chloride, hydrogen carbonate, calcium, magnesium and sulfate ions as shown in Figure 4.13. The interference from all anions was non-significant to the cathodic current signal of NO_3^-, possibly because they are more hydrophilic based on Hofmeister series, allowing nitrate to easily reach the electrode surface (Wang et al., 2013). This indicates that the developed sensor was selective towards nitrate ions and thus can efficiently work in various media.

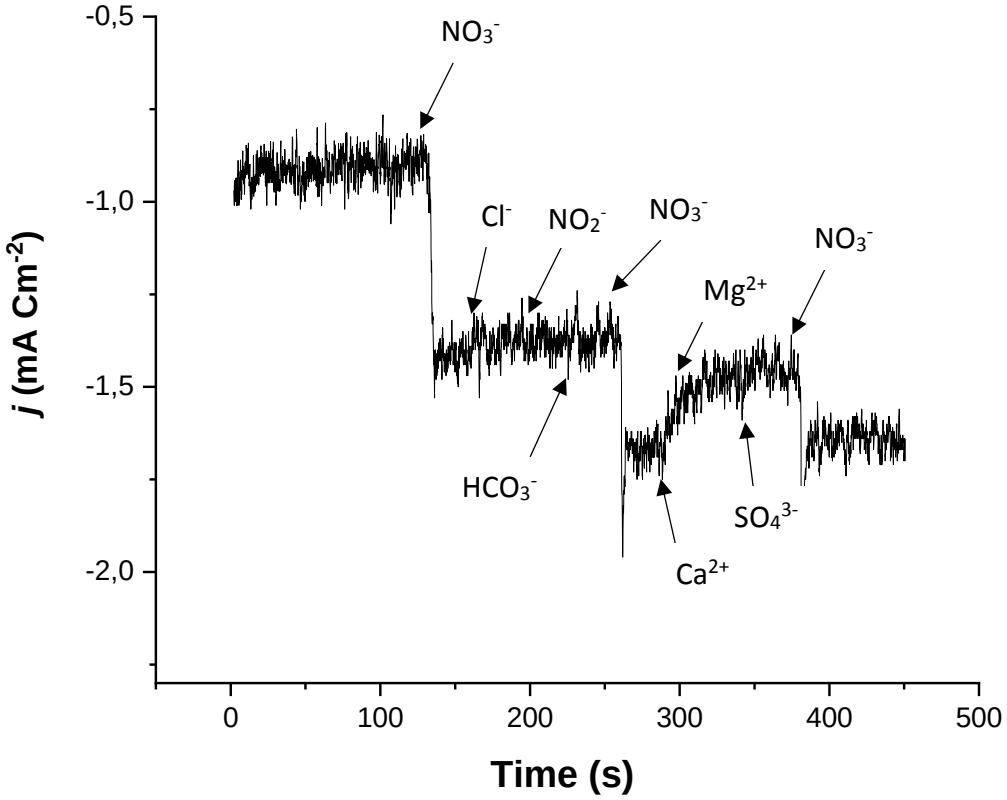

Figure 4.14: Interference in the presence of 5-times higher concentrations of possibly interfering anions present in water

4.3.3.3 Figures of Merit

In order to show the good performance of the currently developed nitrate sensor compared with previously designed sensors based on various nanomaterials, Table 4.2 lists useful data of different nitrate sensors. It thus can be concluded that the currently developed Sn-Cu_xO sensor is comparatively better in terms of its higher sensitivity, linear range and lower limit of detection.

Table 4.4: Sensor performances compared with other reported electrochemical sensors for nitrate detection

Material	Linear Range (uM)	Sensitivity (uA/mM.cm^2)	LOD (uM)	References
Ag NPs/PMA	0-20000	130	-	(Bonyani et al., 2016)
Cu NWs	8-5860	1,375	1,35	(Liang et al., 2016)
Pd-Au NPs	1 000-15000	4,7	-	(Shanshan et al, 2019)
Pd NCs-PPy	-	0,124	0,7444	(Mahmoudian et al, 2015)
ZnO NPs	100-2000	39,91	10	(Gumpu et al., 2017)
Ag@IronOxide	-	663	30	(Bonyani et al, 2015)
Ag NPs/Au	10−10000	-	10	(Alahi and Mukhopadhyay, 2018)
Gr/Cu	9−940	0, 173	10	(Alahi and Mukhopadhyay, 2018)
Gr/Cu NPs/Au	10−90	0.20	7.89	(Alahi and Mukhopadhyay, 2018)
Pd-Sn composite	16−322.6	24.67	3.06	(Alahi and Mukhopadhyay, 2018)
Pd-Au NPs composite	16−242	0.29	1.19	(Alahi and Mukhopadhyay, 2018)
Sn-Cu_xO/FTO	0.01 - 15000	100.3	0.04	This work

4.3.4 Reproducibility, stability, and shelf life

4.3.4.1 Reproducibility

To investigate the practical usage of the developed Sn-Cu_xO NPs modified FTO sensor, the reproducibility of 4 independent fabricated modified electrodes were tested using four CVs run in 0.1M KOH electrolyte solution containing 1mM nitrate solution as shown in Figure 4.14. The relative standard deviation (RSD) of the sensor current responses to 1mM of nitrate was obtained to be 2.64 %, and this small value verifies the high and good reproducibility of the developed electrode. Furthermore, the shelf life of the sensor was studied over a one-month period with the Sn-Cu_xO-FTO electrode tested twice per week. The results showed an RSD value of 4.7 %, which confirms the good durability of the sensor. The electrochemical stability of the as prepared sensor was investigated over 10 repetitive CV scans, and no additional peaks were found.

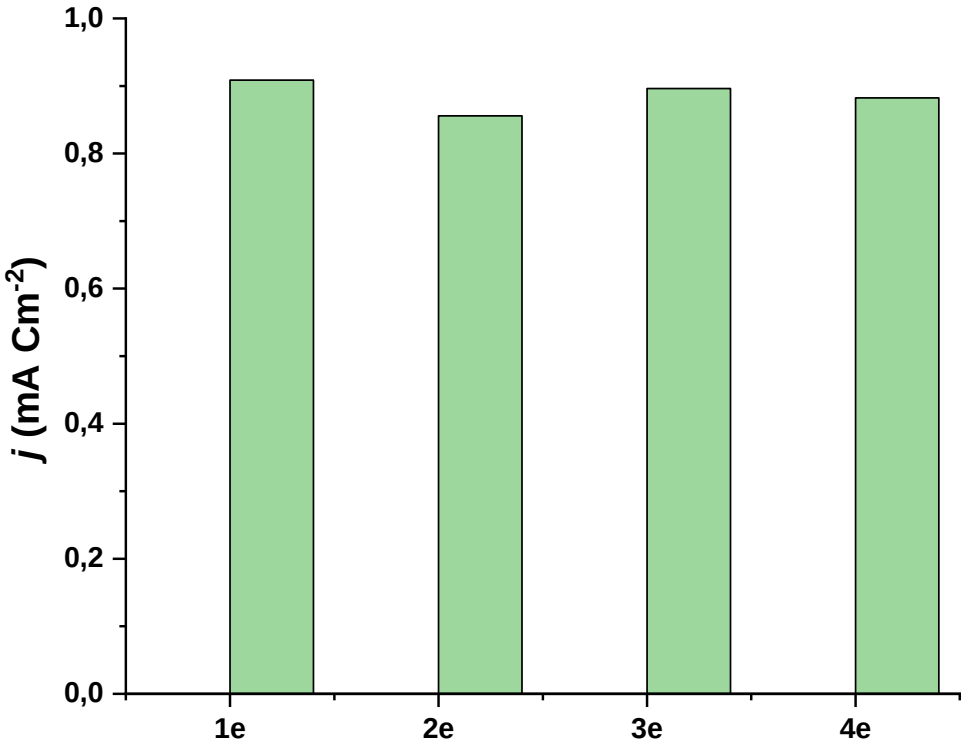

Figure 4.15 : Reproducibility

4.3.4.2 Stability

To investigate the electrochemical stability of the as prepared Sn-Cu_xO sensor for detection of nitrate, the sensors were run over 10 repetitive CV scans, and no additional peaks were found. Thus being stable (figure 4.15).

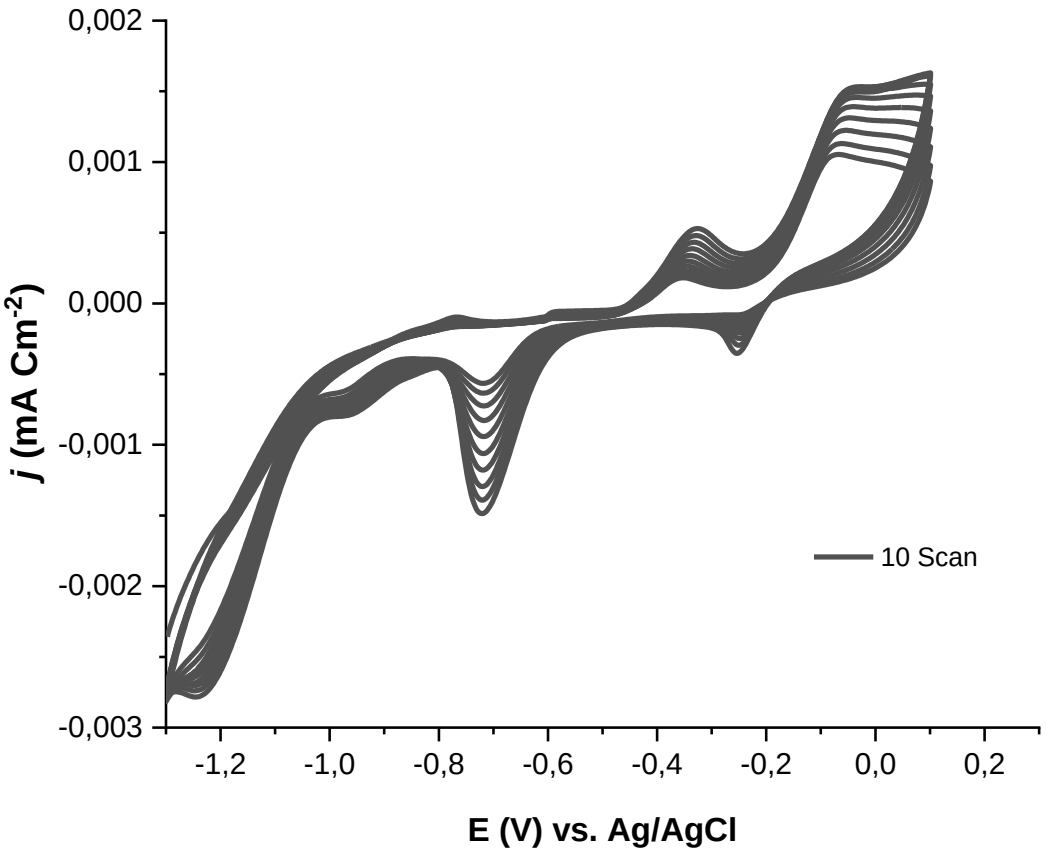

Figure 4.16: Stability

4.3.4.3 Shelf life

The shelf life of the sensor was studied over a one-month period with the Sn-Cu_xO-FTO electrode tested twice per week. The results showed an RSD value of 4.7 %, which confirms the good durability of the sensor (figure 4.16).

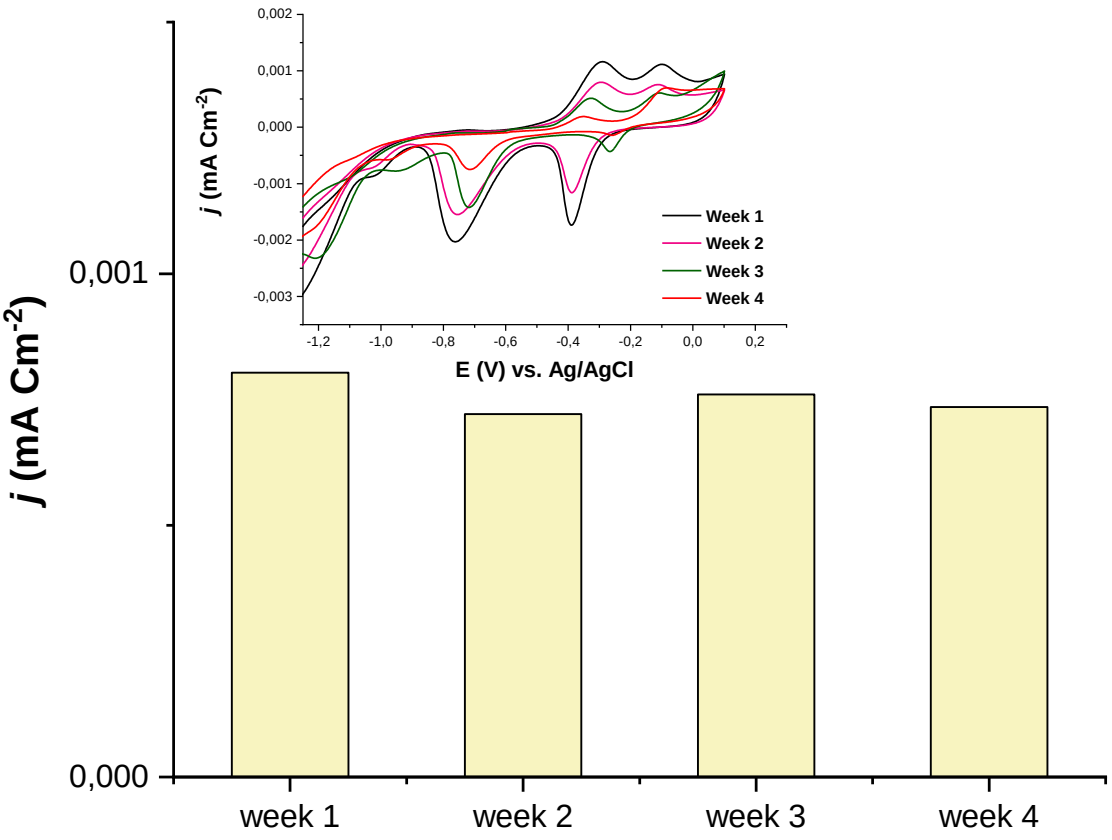

Figure 4.17: Shelf life

4.3.5 Electrochemical impedance spectroscopy (EIS)

The EIS measurements were studied using a three-electrode setup controlled by the Metrohm Autolab PGSTAT204 potentiostat with pre-installed NOVA 2.1 software. EIS data were performed and used to follow the charge-transfer resistances (R_{ct}) changes of the Sn-Cu_xO and Cu_xO electrodes occurring at the interface of their surface modification during electrolysis.

From the shape of an impedance spectrum, the electron transfer kinetics and the diffusion characteristics can be determined. In EIS studies, the semicircle portion at high frequency region represents the electron transfer resistance (Rct) of the electrode, and the linear part at lower frequencies indicates the diffusion limited process. EIS study was conducted using 5mM K_4 [Fe (CN) $_6$]/K_3 [Fe (CN) $_6$] as a redox probe in 0.1M KCl within the frequency range of 1 - 100 KHz, and 100 mV voltage amplitude. Figure… shows the Nyquist plots of Cu_xO and Sn-Cu_xO thin films obtained at the formal potential of 0.205 V (vs. Ag/AgCl reference electrode).

In the Nyquist diagram, the diameter of the semicircle defines the electron transfer resistance (Rct). It shows that the Sn-Cu_xO electrode exhibits a samller diameter (Rct = 50 Ω) which indicates a fast rate transfer compared to that of the Cu_xO electrode (Rct= 70 Ω).

EIS Spectrum Analyser software (ABC Chemistry) was used to fit the EIS data using equivalent circuit modelling (See the Randles equivalent circuits in Figure 4.18). The decreased charge-transfer resistance of Sn-Cu_xO thin film was attributed to the excess free electrons from the Sn doping, which participated in electronic conductivity. The preceding statement agreed with the increased electron-transfer rate of Sn-Cu_xO thin film compared to that of Cu_xO thin film.

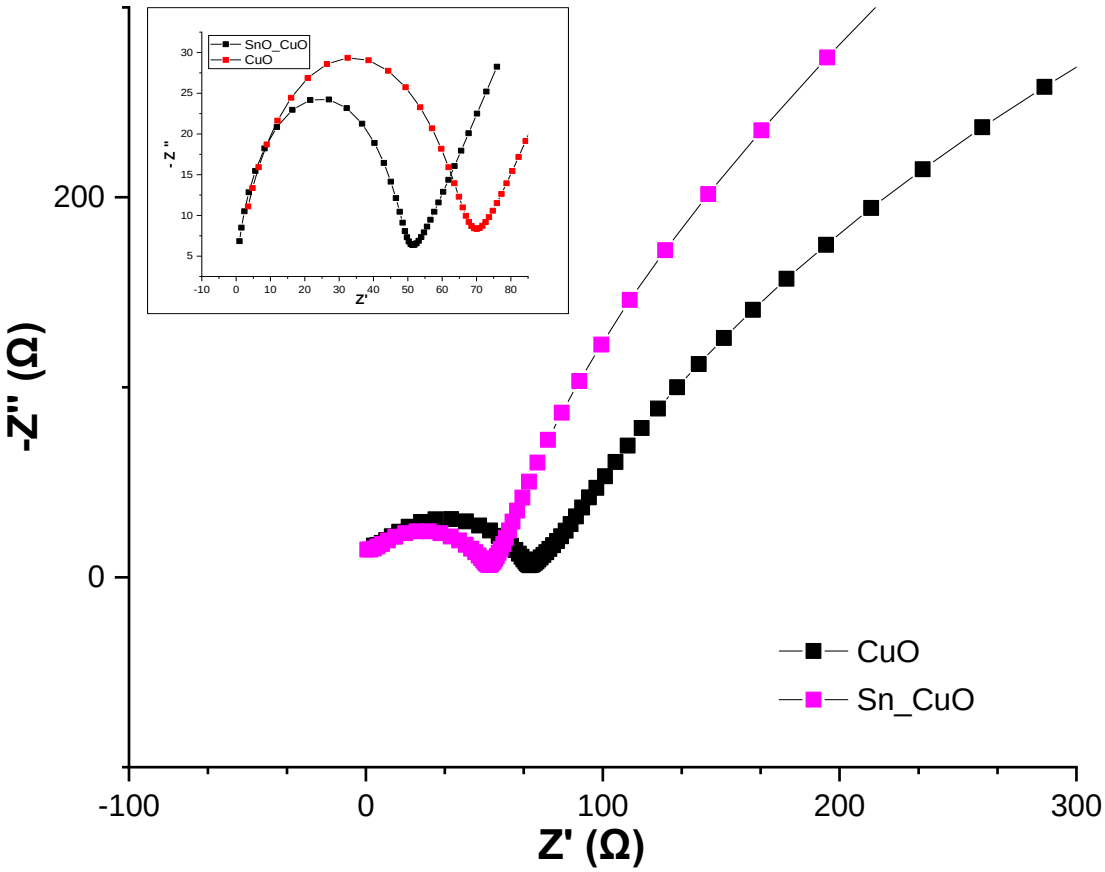

Figure 4.18: EIS Nyquist plots of Cu_xO and Sn-Cu_xO thin films at the formal potential of 0.205 V (vs. Ag/AgCl reference electrode).

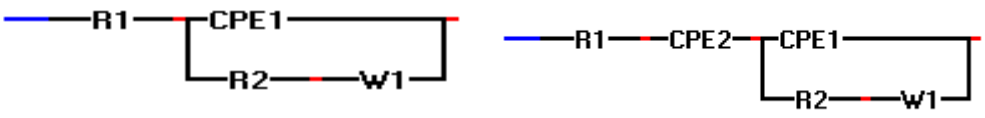

Figure 4.19: EIS Randles equivalent circuits of Sn-Cu_xO thin film

4.3.6 Determination of nitrate in real sample

The recovery study of nitrate in real matrices, such as bore hole water, Mowbray river water, and tap water was conducted using a standard addition method to demonstrate the practical application of the Sn-Cu_xO sensor. The test results are summarized in Table 3. It can be concluded that the Sn-Cu_xO sensor showed good recovery in the range of 97.80 - 111.20 %.

Table 4.5: Real sample data.

Sample	Amount Spiked (mmol)	Amount detected (mmol)	Recovery (%)
Bore hole water	5	5, 19	103, 95
Mowbray River water	5	5, 56	111, 14
Tap water	5	4, 89	97, 8

4.4 Conclusion

In conclusion, this chapter presents a comprehensive analysis of the results obtained from the experimentation involving the synthesis and characterization of Sn-Cu_xO nanocomposite thin films for electro catalytic nitrate detection. Various techniques, including X-ray diffraction (XRD), scanning electron microscopy (SEM), and X-ray photoelectron spectroscopy (XPS), were employed for the physical characterization of the catalysts. The XRD patterns confirmed the successful incorporation of Sn into the Cu_xO lattice, leading to significant crystallographic changes in the Sn-Cu_xO thin film. SEM analysis revealed alterations in surface morphology, indicating structural changes and a decrease in crystallinity after Sn doping.

XPS analysis provided insights into the surface chemistry, confirming the presence of both Cu_2O and CuO phases in the Cu_xO thin film and revealing notable spectral changes upon Sn doping. The electro catalytic performance of the Sn-Cu_xO/FTO electrode was evaluated through cyclic voltammetry (CV) and chronoamperometry (CA) studies. The results demonstrated enhanced electrocatalytic activity for nitrate reduction compared to pristine Cu_xO, attributed to the incorporation of Sn, which introduced excess surface free electrons.

The sensor exhibited a wide linear range (0.01 - 15000 µM) and a low limit of detection (0.04 µM). The chronoamperometric study confirmed the sensor's practical application for nitrate detection, showing good sensitivity and a linear response. Interference studies demonstrated the selectivity of the Sn-Cu_xO sensor towards nitrate ions.

The sensor's performance was compared with other reported electrochemical sensors for nitrate detection, highlighting its superior sensitivity, linear range, and lower limit of detection. Reproducibility, stability, and shelf life studies further validated the sensor's practicality and reliability, with low relative standard deviation values.

Chapter 5 : Conclusion & Recommendations

5.1 Introduction

Nitrate detection is a crucial aspect of environmental monitoring, water quality evaluation, and agricultural activities. Water with excessive nitrate levels can be harmful to both the environment and human health. A number of techniques are used to detect nitrate, and one of these techniques uses specialized sensors to do amperometric detection. The method should be sensitive enough to detect low concentrations of nitrate, and selective in the presence of additional ions. An improved nitrate sensor based on tin doped copper oxide (Sn-doped Cu_xO) thin films modified fluorine tin oxide (FTO) electrode was constructed for the amperometric detection of nitrate. In this chapter, a summary and conclusions of the work done was presented as well as some contributions and recommendations.

5.2 Conclusion

We have successfully prepared a Sn-doped Cu_xO (Cu_2O and CuO) thin film via spin-coating metal-organic decomposition for characterization and detection of nitrate. Nitrate electro reduction at Cu_xO was found to be mediated by the Cu/Cu_2O couple and turned out to be a one-electron transfer process with NO_2 as the reduction product.

In this chapter, a comprehensive analysis of the experimental results and characterization of Cu_xO and Sn-doped Cu_xO nanocomposite thin films as electrocatalysts for nitrate detection has been presented. Various techniques, including X-ray diffraction (XRD), scanning electron microscopy (SEM), and X-ray photoelectron spectroscopy (XPS), were employed for the physical characterization of the catalysts. The study revealed the successful incorporation of Sn_4^+ into the lattice structure of Cu_xO, resulting in significant crystallographic changes, such as enhanced growth of CuO, peak splitting, and the disappearance of certain XRD peaks.

SEM images displayed clear changes in the surface morphology of the Cu_xO/FTO electrode upon Sn doping, indicating structural alterations and reduced crystallinity. XPS analysis provided insights into the surface chemistry, confirming the presence of both Cu_2O and CuO phases in the Cu_xO thin film, and showcasing spectral changes after Sn doping. The findings suggested a decrease in the number of Cu_2^+ ions and the generation of Cu_{2+}^-vacancies upon Sn doping, contributing to the enhanced growth of CuO.

The electro catalytic performance of the as-prepared electrodes was evaluated through cyclic voltammetry (CV) studies. Sn-doped Cu_xO exhibited superior electro catalytic response for nitrate detection compared to pristine CuxO, attributed to the incorporation of Sn, which supplied surface free electrons enhancing the conduction during nitrate electro-reduction. The CV curves demonstrated the sensitivity of Sn-doped Cu_xO to nitrate concentration, with a linear increase in cathodic peak current.

Chronoamperometry (CA) studies further confirmed the nitrate-sensing capability of Sn-doped Cu_xO, exhibiting a linear response to consecutive additions of nitrate. The sensor showed excellent selectivity, as interference from other anions was non-significant. The Sn-doped Cu_xO sensor demonstrated impressive sensitivity of 100.27 $\mu A.mM^{-1}.cm^{-2}$ at a potential of -1 V (vs. Ag/AgCl), a linear concentration range of up to 15 mM, a fast response time of < 5 s, and a low limit of detection of 0.04 µM that outperformed those in the reported literature above, making it suitable for practical applications.

The sensor's reproducibility, stability, and shelf life were assessed, revealing good reproducibility with a relative standard deviation of 2.64%, stability over 10 repetitive CV scans, and a shelf life of one month with an RSD value of 4.7%. Additionally, an electrochemical impedance spectroscopy (EIS) study provided insights into the charge-transfer resistances changes occurring at the electrode interface during electrolysis.

In conclusion, the study demonstrates the successful synthesis and characterization of Sn-CuxO nanocomposite thin films and their application as effective electrocatalysts for nitrate detection. The developed sensor exhibits excellent performance characteristics, making it a promising candidate for practical applications in environmental monitoring and water quality assessment.

5.3 Contribution

This research fabricated a Sn-Cu_xO electrochemical sensor using a cost effective method named electrochemical technique as mentioned in the literature above as compared to the conventionally utilized method. The sensor was found to be selective, sensitive and having a

lower limit of detection towards nitrate making it useful in catalysis applications and chemical processes. It may find applications in diverse fields in particular in gas sensing.

5.4 Recommendations

This research focused on the development and catalytic performance of the Sn-Cu_xO electrochemical sensor in aqueous systems in order to detect nitrate ions. The objectives were achieved. However, recommending directions for further study directs the field toward filling up knowledge gaps and advancing understanding:

- Incorporating Sn-Cu_xO with other materials or nanostructures to achieve synergistic effects and improved sensing properties,
- Investigating the impact of different nanostructures (e.g., nanoparticles, nanowires) on the sensor's performance and explore their influence on sensitivity and response time,
- Examining the feasibility of adding more sensing components to the Sn-Cu_xO nanocomposite.

Bibliography

AAZADFAR, P., SOLATI, E. & DORRANIAN, D. 2018. Properties of Au/Copper oxide nanocomposite prepared by green laser irradiation of the mixture of individual suspensions. *Optical Materials,* 78**,** 388-395.

ABUELWAFA, A. A., EL-SADEK, M. S. A., ELNOBI, S. & SOGA, T. 2021. Effect of transparent conducting substrates on the structure and optical properties of tin (II) oxide (SnO) thin films: Comparative study. *Ceramics International,* 47**,** 13510-13518.

ADLAKHA-HUTCHEON, G., KHAYDAROV, R., KORENSTEIN, R., VARMA, R., VASEASHTA, A., STAMM, H. & ABDEL-MOTTALEB, M. 2009. Nanomaterials, Nanotechnology. *In:* LINKOV, I. & STEEVENS, J. (eds.) *Nanomaterials: Risks and Benefits.* Dordrecht: Springer Netherlands.

AHMED, A., ROBERTSON, C. M., STEINER, A., WHITTLES, T., HO, A., DHANAK, V. & ZHANG, H. 2016. Cu(i)Cu(ii)BTC, a microporous mixed-valence MOF via reduction of HKUST-1. *RSC Advances,* 6**,** 8902-8905.

ALAHI, M. E. E. & MUKHOPADHYAY, S. C. 2018. Detection methods of nitrate in water: A review. *Sensors and Actuators A: Physical,* 280**,** 210-221.

ALAM, M. M., ABUL HASNAT, M., RASHED, M. A., NIZAM UDDIN, S., RAHMAN, M., AMERTHARAJ, S., AHMED, N. & MOHAMED, N. 2015. Nitrate detection activity of Cu particles deposited on pencil graphite by fast scan cyclic voltammetry. *Journal of Analytical Chemistry,* 70.

AMALI, R. K. A., LIM, H. N., IBRAHIM, I., HUANG, N. M., ZAINAL, Z. & AHMAD, S. A. A. 2021. Significance of nanomaterials in electrochemical sensors for nitrate detection: A review. *Trends in Environmental Analytical Chemistry,* 31**,** e00135.

AMERTHARAJ, S., HASNAT, M. A. & MOHAMED, N. 2014. Electroreduction of nitrate ions at a platinum-copper electrode in an alkaline medium: Influence of sodium inositol phytate. *Electrochimica Acta,* 136**,** 557-564.

AOUINA, N., CACHET, H., DEBIEMME-CHOUVY, C. & TRAN, T. T. M. 2010. Insight into the electroreduction of nitrate ions at a copper electrode, in neutral solution, after determination of their diffusion coefficient by electrochemical impedance spectroscopy. *Electrochimica Acta,* 55**,** 7341-7345.

ARISTOV, N. & HABEKOST, A. 2015. Cyclic voltammetry-A versatile electrochemical method investigating electron transfer processes. *World J. Chem. Educ,* 3**,** 115-119.

ASKHAM, T. M. & VAN DER POLL, H. M. 2017. Water Sustainability of Selected Mining Companies in South Africa. *Sustainability,* 9**,** 957.

BALıK, M., BULUT, V. & ERDOGAN, I. Y. 2019. Optical, structural and phase transition properties of Cu2O, CuO and Cu2O/CuO: Their photoelectrochemical sensor applications. *International Journal of Hydrogen Energy,* 44**,** 18744-18755.

BANSOD, B. K. S., KUMAR, T. S. S., THAKUR, R., RANA, S. & SINGH, I. 2017. A review on various electrochemical techniques for heavy metal ions detection with different sensing platforms. *Biosensors & bioelectronics,* 94**,** 443-455.

BATURAY, Ş., TOMBAK, A., BATIBAY, D. & OCAK, Y. S. 2019. n-Type conductivity of CuO thin films by metal doping. *Applied Surface Science,* 477**,** 91-95.

BIN MOBARAK, M., HOSSAIN, M. S., CHOWDHURY, F. & AHMED, S. 2022. Synthesis and characterization of CuO nanoparticles utilizing waste fish scale and exploitation of XRD peak profile analysis for approximating the structural parameters. *Arabian Journal of Chemistry,* 15**,** 104117.

BOMMIREDDY, N. & PALATHEDATH, S. K. 2020. Templated bimetallic copper-silver nanostructures on pencil graphite for amperometric detection of nitrate for aquatic monitoring. *Journal of Electroanalytical Chemistry,* 856**,** 113660.

BONYANI, M., MIRZAEI, A., LEONARDI, S. G. & NERI, G. 2016. Silver nanoparticles/polymethacrylic acid (AgNPs/PMA) hybrid nanocomposites-modified electrodes for the electrochemical detection of nitrate ions. *Measurement,* 84**,** 83-90.

CARPENTER, N. G. & PLETCHER, D. 1995. Amperometric method for the determination of nitrate in water. *Analytica Chimica Acta,* 317**,** 287-293.

CHANDRASEKARAN, S. 2013. A novel single step synthesis, high efficiency and cost effective photovoltaic applications of oxidized copper nano particles. *Solar Energy Materials and Solar Cells,* 109**,** 220-226.

CIFTYÜREK, E., ŠMÍD, B., LI, Z., MATOLÍN, V. & SCHIERBAUM, K. 2019. Spectroscopic Understanding of SnO2 and WO3 Metal Oxide Surfaces with Advanced Synchrotron Based; XPS-UPS and Near Ambient Pressure (NAP) XPS Surface Sensitive Techniques for Gas Sensor Applications under Operational Conditions. *Sensors,* 19**,** 4737.

CLAASEN, T. & LEWIS, E. W. 2017. Nitrate and bacteriological assessment of groundwater in Omaheke region, Namibia.

CLIMENT, V. & FELIU, J. M. 2018. Cyclic Voltammetry. *In:* WANDELT, K. (ed.) *Encyclopedia of Interfacial Chemistry.* Oxford: Elsevier.

ESSER, M., ROHDE, G. & REHTANZ, C. 2022. Electrochemical Impedance Spectroscopy Setup based on Standard Measurement Equipment. *Journal of Power Sources,* 544**,** 231869.

FAJERWERG, K., YNAM, V., CHAUDRET, B., GARÇON, V., THOURON, D. & COMTAT, M. 2010. An original nitrate sensor based on silver nanoparticles electrodeposited on a gold electrode. *Electrochemistry Communications,* 12**,** 1439-1441.

FAN, H. & KIM, H.-E. 2001. Perovskite stabilization and electromechanical properties of polycrystalline lead zinc niobate–lead zirconate titanate. *Journal of Applied Physics,* 91**,** 317-322.

FELIX, S., GRACE, A. N. & JAYAVEL, R. 2018. Sensitive electrochemical detection of glucose based on Au-CuO nanocomposites. *Journal of Physics and Chemistry of Solids,* 122**,** 255-260.

FOX, C. & BRESLIN, C. 2020. Electrochemical formation of silver nanoparticles and their applications in the reduction and detection of nitrates at neutral pH. *Journal of Applied Electrochemistry,* 50.

FU, Y., BIAN, C., KUANG, J., WANG, J., TONG, J. & XIA, S. 2015. A palladium-tin modified microband electrode array for nitrate determination. *Sensors,* 15**,** 23249-23261.

GIL, R. L., AMORIM, C. G., MONTENEGRO, M. C. B. S. M. & ARAÚJO, A. N. 2019. Potentiometric detection in liquid chromatographic systems: An overview. *Journal of Chromatography A,* 1602**,** 326-340.

GUMPU, M. B., NESAKUMAR, N., RAMACHANDRA, B. L. & RAYAPPAN, J. B. B. 2017. Zinc oxide nanoparticles-based electrochemical sensor for the detection of nitrate ions in water with a low detection limit—a chemometric approach. *Journal of Analytical Chemistry,* 72**,** 316-326.

GUTIÉRREZ, M., BIAGIONI, R. N., ALARCÓN-HERRERA, M. T. & RIVAS-LUCERO, B. A. 2018. An overview of nitrate sources and operating processes in arid and semiarid aquifer systems. *Science of The Total Environment,* 624**,** 1513-1522.

HAMMOUDA, N. & KAMEL, B. 2020. EIS study of the corrosion behavior of an organic coating applied on Algerian oil tanker. *Metallurgical Research & Technology,* 117**,** 610.

HEYDARI, H., GHOLIVAND, M. B. & ABDOLMALEKI, A. 2016. Cyclic voltammetry deposition of copper nanostructure on MWCNTs modified pencil graphite electrode: An ultra-sensitive hydrazine sensor. *Materials Science and Engineering: C,* 66**,** 16-24.

JAHN, B. R., LINKER, R., UPADHYAYA, S. K., SHAVIV, A., SLAUGHTER, D. C. & SHMULEVICH, I. 2006. Mid-infrared Spectroscopic Determination of Soil Nitrate Content. *Biosystems Engineering,* 94**,** 505-515.

JASNA, R. S., GANDHIMATHI, R., LAVANYA, A. & RAMESH, S. T. 2020. An integrated electrochemical-adsorption system for removal of nitrate from water. *Journal of Environmental Chemical Engineering,* 8**,** 104387.

KIM, K., KIM, K. L. & SHIN, K. S. 2012. Selective detection of aqueous nitrite ions by surface-enhanced Raman scattering of 4-aminobenzenethiol on Au. *Analyst,* 137**,** 3836-3840.

KODAMATANI, H., YAMAZAKI, S., SAITO, K., TOMIYASU, T. & KOMATSU, Y. 2009. Selective determination method for measurement of nitrite and nitrate in water samples using high-performance liquid chromatography with post-column photochemical reaction and chemiluminescence detection. *Journal of Chromatography A,* 1216**,** 3163-3167.

KUANG, P., NATSUI, K. & EINAGA, Y. 2018. Comparison of performance between boron-doped diamond and copper electrodes for selective nitrogen gas formation by the electrochemical reduction of nitrate. *Chemosphere,* 210**,** 524-530.

LARSON, R. G. & REHG, T. J. 1997. Spin Coating. *In:* KISTLER, S. F. & SCHWEIZER, P. M. (eds.) *Liquid Film Coating: Scientific principles and their technological implications.* Dordrecht: Springer Netherlands.

LI, G., YUAN, H., MOU, J., DAI, E., ZHANG, H., LI, Z., ZHAO, Y., DAI, Y. & ZHANG, X. 2022. Electrochemical detection of nitrate with carbon nanofibers and copper co-modified carbon fiber electrodes. *Composites Communications,* 29**,** 101043.

LIANG, J., ZHENG, Y. & LIU, Z. 2016. Nanowire-based Cu electrode as electrochemical sensor for detection of nitrate in water. *Sensors and Actuators B: Chemical,* 232**,** 336-344.

LUNDBERG, J. O., FEELISCH, M., BJÖRNE, H., JANSSON, E. A. & WEITZBERG, E. 2006. Cardioprotective effects of vegetables: is nitrate the answer? *Nitric Oxide,* 15**,** 359-62.

MASINDI, V. & FOTEINIS, S. 2021. Groundwater contamination in sub-Saharan Africa: Implications for groundwater protection in developing countries. *Cleaner Engineering and Technology,* 2**,** 100038.

MAURO, J. C. 2021. Chapter 3 - Fick's Laws of Diffusion. *In:* MAURO, J. C. (ed.) *Materials Kinetics.* Elsevier.

MOHEBBI, S., MOLAEI, S. & JUDY AZAR, A. R. 2013. Preparation and study of Sn-doped CuO nanoparticles as semiconductor. *J. Appl. Chem.,* 8**,** 27-30.

MUMTARIN, Z., RAHMAN, M. M., MARWANI, H. M. & HASNAT, M. A. 2020. Electro-kinetics of conversion of NO3− into NO2−and sensing of nitrate ions via reduction reactions at copper immobilized platinum surface in the neutral medium. *Electrochimica Acta,* 346**,** 135994.

NDALA, A., ITOTA, B., CHAMIER, J., RAY, S., SUNDAY, C. & CHOWDHURY, M. 2021. Novel (CH6N3+, NH3+)-functionalized and nitrogen doped Co3O4 thin film electrochemical sensor for nanomolar detection of nitrite in neutral pH. *Electrochimica Acta,* 388**,** 138556.

PAL, M., PAL, U., JIMÉNEZ, J. M. G. Y. & PÉREZ-RODRÍGUEZ, F. 2012. Effects of crystallization and dopant concentration on the emission behavior of TiO2:Eu nanophosphors. *Nanoscale Research Letters,* 7**,** 1.

PETROVIC, S., RAJČIĆ-VUJASINOVIĆ, M., STEVIC, Z. & GREKULOVI, V. 2011. Cuprous Oxide as an Active Material for Solar Cells.

RAJA, P. B., MUNUSAMY, K. R., PERUMAL, V. & IBRAHIM, M. N. M. 2022. 5 - Characterization of nanomaterial used in nanobioremediation. *In:* IQBAL, H. M. N., BILAL, M. & NGUYEN, T. A. (eds.) *Nano-Bioremediation : Fundamentals and Applications.* Elsevier.

RAMAKRISHNAPPA, T., SURESHKUMAR, K. & PANDURANGAPPA, M. 2020. Copper oxide impregnated glassy carbon spheres based electrochemical interface for nitrite/nitrate sensing. *Materials Chemistry and Physics,* 245**,** 122744.

SABERIAN-BORUJENI, M., JOHARI-AHAR, M., HAMZEIY, H., BARAR, J. & OMIDI, Y. 2014. Nanoscaled aptasensors for multi-analyte sensing. *BioImpacts: BI,* 4**,** 205.

SEDENHO, G. C., PAIM, L. L. & STRADIOTTO, N. R. 2013. Simple and direct potentiometric determination of potassium ions in biodiesel microemulsions at a glassy carbon electrode modified with nickel(ii) hexacyanoferrate nanoparticles. *Analytical Methods,* 5**,** 4145-4151.

SHANG, Y. & GUO, L. 2015. Facet-Controlled Synthetic Strategy of Cu2O-Based Crystals for Catalysis and Sensing. *Advanced Science,* 46.

SIDDIQUI, H., SINGH, N., CHAUHAN, V., SATHISH, N. & KUMAR, S. 2021. Electrochemical 3D printed copper garden for nitrate detection. *Materials Letters,* 305**,** 130795.

SIGUA, G. 2011. Sustainable Cow-Calf Operations and Water Quality.

SIMÕES, F. R. & XAVIER, M. G. 2017. 6 - Electrochemical Sensors. *In:* DA RÓZ, A. L., FERREIRA, M., DE LIMA LEITE, F. & OLIVEIRA, O. N. (eds.) *Nanoscience and its Applications.* William Andrew Publishing.

SINDELAR, J. J. & MILKOWSKI, A. L. 2012. Human safety controversies surrounding nitrate and nitrite in the diet. *Nitric Oxide,* 26**,** 259-66.

SOHAIL, M. & ADELOJU, S. B. 2016. Nitrate biosensors and biological methods for nitrate determination. *Talanta,* 153**,** 83-98.

SOYOON, S., RAMADOSS, A., SARAVANAKUMAR, B. & KIM, S. J. 2014. Novel Cu/CuO/ZnO hybrid hierarchical nanostructures for non-enzymatic glucose sensor application. *Journal of Electroanalytical Chemistry,* 717-718**,** 90-95.

STORTINI, A. M., MORETTO, L. M., MARDEGAN, A., ONGARO, M. & UGO, P. 2015. Arrays of copper nanowire electrodes: Preparation, characterization and application as nitrate sensor. *Sensors and Actuators B: Chemical,* 207**,** 186-192.

STRLE, D., STEFANE, B., ZUPANIČ, E., TRIFKOVIČ, M., MAČEK, M., JAKŠA, G., KVASIC, I. & MUŠEVIČ, I. 2014. Sensitivity Comparison of Vapor Trace Detection of Explosives Based on Chemo-Mechanical Sensing with Optical Detection and Capacitive Sensing with Electronic Detection. *Sensors (Basel, Switzerland),* 14**,** 11467-11491.

STUDER, A. & CURRAN, D. P. 2014. The electron is a catalyst. *Nature Chemistry,* 6**,** 765-773.

SURESH, G., XIONG, W., ROUISSI, T. & BRAR, S. K. 2019. Nitrates. *In:* MELTON, L., SHAHIDI, F. & VARELIS, P. (eds.) *Encyclopedia of Food Chemistry.* Oxford: Academic Press.

THIAGARAJAN, S., SANMUGAM, A. & VIKRAMAN, D. Facile Methodology of Sol-Gel Synthesis for Metal Oxide Nanostructures. 2017.

TOKTAREV, A. V. & ECHEVSKII, G. V. 2008. Hofmeister Anion Effect on the Formation of Zeolite Beta. *In:* GÉDÉON, A., MASSIANI, P. & BABONNEAU, F. (eds.) *Studies in Surface Science and Catalysis.* Elsevier.

TYAGI, S., RAWTANI, D., KHATRI, N. & THARMAVARAM, M. 2018. Strategies for Nitrate removal from aqueous environment using Nanotechnology: A Review. *Journal of Water Process Engineering,* 21**,** 84-95.

VADDIRAJU, S., TOMAZOS, I., BURGESS, D. J., JAIN, F. C. & PAPADIMITRAKOPOULOS, F. 2010. Emerging synergy between nanotechnology and implantable biosensors: A review. *Biosensors and Bioelectronics,* 25**,** 1553-1565.

WANG, Q.-H., YU, L.-J., LIU, Y., LIN, L., LU, R.-G., ZHU, J.-P., HE, L. & LU, Z.-L. 2017. Methods for the detection and determination of nitrite and nitrate: A review. *Talanta,* 165**,** 709-720.

WANG, T., SCHLUETER, K. T., RIEHL, B. L., JOHNSON, J. M. & HEINEMAN, W. R. 2013. Simplified Nitrate-Reductase-Based Nitrate Detection by a Hybrid Thin-Layer Controlled Potential Coulometry/Spectroscopy Technique. *Analytical Chemistry,* 85**,** 9486-9492.

WANG, X., HU, C., LIU, H., DU, G., HE, X. & XI, Y. 2010. Synthesis of CuO nanostructures and their application for nonenzymatic glucose sensing. *Sensors and Actuators B: Chemical,* 144**,** 220-225.

WANG, Y., LIU, J. & XIA, C. 2011. Insights into Supported Copper(II)-Catalyzed Azide-Alkyne Cycloaddition in Water. *Advanced Synthesis & Catalysis,* 353**,** 1534-1542.

WHITMORE, W. F. & LAURO, M. 2002. Metallic soaps-Their Uses, Preparation and Properties. Available: http://pubs.acs.org [Accessed June 01].

YANG, Q. & ZHAO, L. R. 2008. Characterization of nano-layered multilayer coatings using modified Bragg law. *Materials Characterization,* 59**,** 1285-1291.

ŽABČÍKOVÁ, S., VU, L., CERVENKA, L., TAMBOR, V. & VAŠATOVÁ, M. 2016. Determination of ascorbic acid in pharmaceutical preparation and fruit juice using modified carbon paste electrode. *Potravinarstvo,* 10.

ZENG, D. W., YUNG, K. C. & XIE, C. S. 2003. UV Nd:YAG laser ablation of copper: chemical states in both crater and halo studied by XPS. *Applied Surface Science,* 217**,** 170-180.

https://www.researchgate.net/figure/WHO-drinking-water-standards-WHO-2011_tbl2_276497542

Appendices

7.1 Appendix A: Extract from the published paper

Two electron transfer mediated enhanced electrochemical nitrate detection by Sn doped CuxO thin film electrode

Ariel Ndala†, Gloria Kibambo†, Orlette Mkhari, Mahabubur Chowdhury*

Nanomaterial research group (NRG), Faculty of Engineering and the Built Environment, Cape Peninsula University of Technology, Bellville-7535, South Africa

†These two Authors contributed equally to this work

*Corresponding author email: chowdhurym@cput.ac.za

Abstract

The unique electrochemical and electronic properties of Cu_xO (Cu_2O/CuO) gives it merit to be used in the development of electronic devices. This paper presents the facile chemical route for the development of a sensitive, accurate, and low-cost nitrate electrochemical sensor based on undoped and Sn-doped Cu_xO thin film electrode. Various characterization techniques were used to study the physical, electro-chemical, and electronic properties of the material. Sn-doping resulted in an increase in the number of electron transfers from 1 to 2 as compared to undoped Cu_xO. The prepared sensor exhibited a high sensitivity of 100.27 µA $mM^{-1}cm^{-2}$, a wide linear concentration range of up to 50 mM, a fast response time of < 5 s was observed at a potential of -1 V (vs. Ag / AgCl), and a very low limit of detection of 0.04 µM (S/N = 3) that outperformed those in the recent literature. The electrode was selective for nitrate in the presence of common interference species and exhibited chemical stability and reproducibility.

Keywords: spin-coating; metal-organic decomposition; Sn-doping; thin films; electrochemical sensor

Figure A0.1: Extract from the published paper derived from this research project

7.2 Appendix B: EIS spectrum analyser

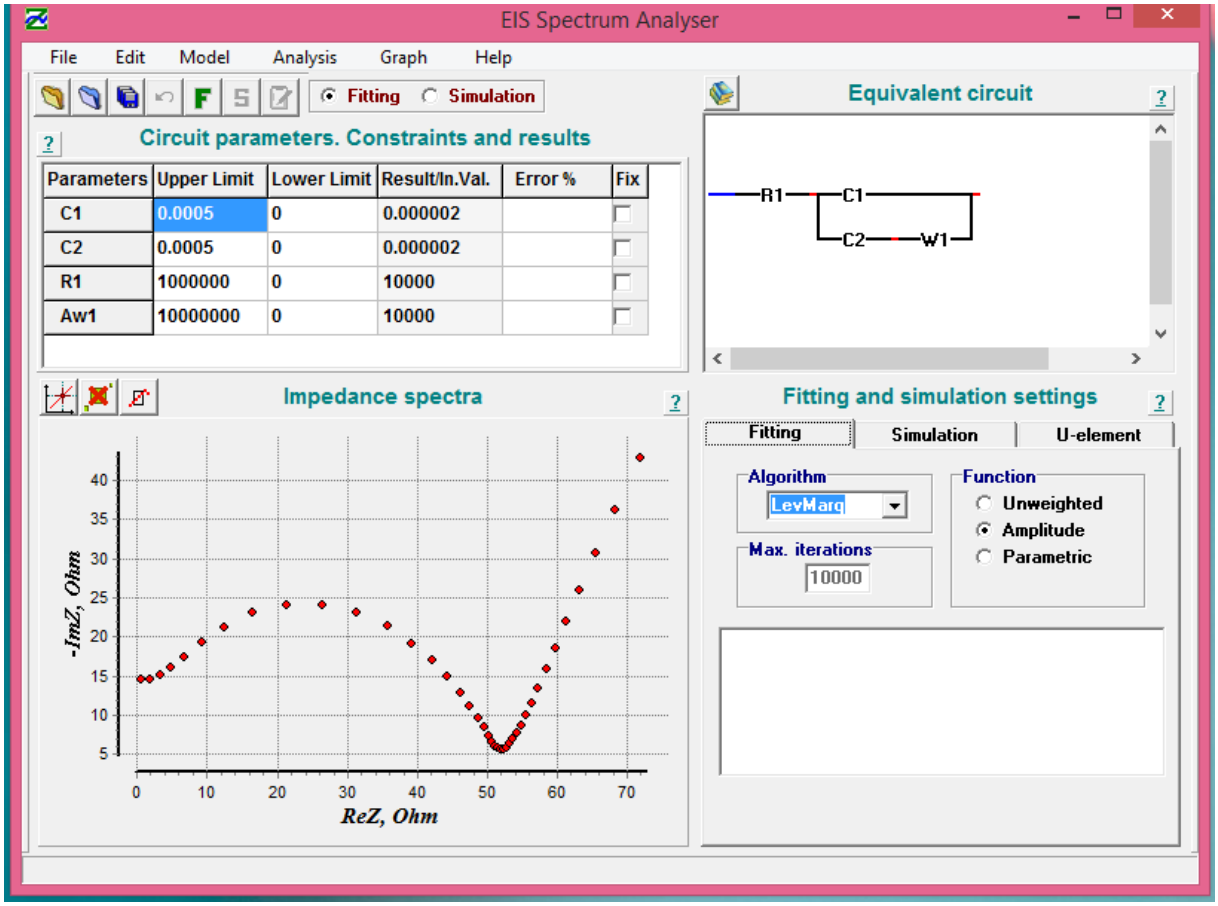

Figure B0.2: EIS Spectrum Analyser